IHF regulates host colonization factors in the bee gut symbiont *Frischella perrara*

K. Schmidt[1,3], S. Leopold-Messer[2], O. Emery[1], Y. El-Chazli[1], T. Steiner[1], J. Piel[2] & P. Engel[1]

1 Department of Fundamental Microbiology, University of Lausanne, Lausanne, Switzerland

2 Institute of Microbiology, Eidgenössische Technische Hochschule (ETH) Zurich, Zürich, Switzerland

3 Current affiliation: Roche Diagnostics International Ltd, Rotkreuz, Switzerland

Correspondence:

Prof. Philipp Engel

Department of Fundamental Microbiology

University of Lausanne, CH-1015 Lausanne, Switzerland

Tel.: +41 (0)21 692 56 12

e-mail: philipp.engel@unil.ch

Abstract

Gut bacteria colonize specific niches in the digestive tract of animals. Yet, the genetic basis of these associations often remains elusive. The gut symbiont *Frischella perrara* colonizes the anterior hindgut of honey bees, where it causes a characteristic immune response leading to the formation of the scab phenotype. Genetic determinants required for the establishment of this specific association are currently unknown. Here, we independently isolated three point mutations in the two genes encoding the DNA-binding protein integration host factor (IHF). The mutations resulted in the formation of larger colonies on agar plates and the absence of an aryl polyene metabolite conferring the yellow color to colonies of *F. perrara*. Inoculation of microbiota-free bees with one of these mutants drastically decreased gut colonization of *F. perrara* and abolished scab development. Using RNAseq we show that IHF affects the expression of potential colonization factors, including a colibactin biosynthetic gene cluster, two Type 6 secretion systems, pili genes, and the aryl polyene biosynthesis pathway. Individual gene deletions of these components revealed different colonization defects indicating that these genetic determinants of *F. perrara* have distinct roles in the interaction with the host. IHF is conserved across many bacteria and may regulate host colonization also in other animal symbionts.

36 **Introduction**

37 The digestive tract of many animals is colonized by specialized gut symbionts that occupy
38 distinct physical niches and utilize diverse nutrients. Owing to the availability of genetic tools,
39 gnotobiotic animal models and multi-omics approaches, we can now study the genetic features
40 that allow gut symbionts to colonize various animal hosts including mammals, fishes, and
41 insects (1-10).

42 The Western honey bee, *Apis mellifera,* is a particularly interesting model to characterize
43 colonization factors of bacterial gut symbionts, due to its agricultural importance and the
44 tractability of its gut microbiota. Honey bees harbor relatively simple yet highly specialized gut
45 microbiota composed of 8-10 bacterial genera (11, 12). The wide distribution of this community
46 across social bees suggests long evolutionary associations with the host (13). Moreover,
47 different members of the bee gut microbiota colonize distinct physical niches along the gut.
48 Lactobacilli and Bifidobacteria predominate in the posterior hindgut (rectum), while
49 Gammaproteobacteria (*Frischella perrara* and *Gilliamella* species) and a betaproteobacterium
50 (*Snodgrassella alvi*) preferentially colonize the anterior hindgut (ileum and adjacent pylorus, i.e.,
51 the transition zone between midgut and ileum) (11, 14-16). The partitioning of these bacteria
52 into distinct gut compartments suggests the existence of specific bacterial mechanisms that
53 facilitate colonization.

54 Most bacteria of the bee gut microbiota can be cultured and experiments with gnotobiotic bees
55 have been established (17-21). Moreover, genomic analyses have provided important insights
56 about the functional potential of bee gut symbionts and their adaptation to the gut environment
57 (21-29). Yet, little is known about which genes are directly involved in establishing colonization
58 in the bee gut and how these genes are regulated. The only symbiont that has been extensively
59 studied in this respect is *S. alvi.* Using transposon sequencing and transcriptome analysis,
60 Powell et al. determined genome-wide host colonization factors in *S. alvi* (7). Most genes with
61 strong fitness effects were found to belong to three major categories: extracellular interactions,
62 metabolism, and stress response. In particular, genes for attachment and biofilm formation were

63 highly beneficial for colonization, which is in agreement with the observation that this gut
64 symbiont adheres to the host epithelium of the ileum and forms a multispecies biofilm with
65 *Gilliamella*.

66 The honey bee gut symbiont *Frischella perrara* belongs to the recently described family
67 Orbaceae within the Gammaproteobacteria (30). It is taxonomically close to the bee gut
68 symbiont *Gilliamella* and also shows a similar metabolism as *Gilliamella* (31). However,
69 compared to the other members of the bee gut microbiota*, F. perrara* shows a rather distinctive
70 colonization phenotype*.* While *S. alvi* and *Gilliamella* have been reported to colonize the host
71 epithelium of the entire ileum (32, 33), *F. perrara* preferentially colonizes the transition zone
72 between the midgut and the ileum, i.e., the pylorus. Moreover, colonization with *F. perrara* leads
73 to the appearance of a brown to black material on the luminal side of the epithelial surface
74 between the cuticle layer of the host tissue and the adherent *F. perrara* cells (34). This so–
75 called scab phenotype forms after 5-7 days post-colonization and has so far not been reported
76 to be triggered by any other gut symbiont than *F. perrara*. Transcriptome analysis of the host
77 showed that *F. perrara* elicits a specific immune response which includes the upregulation of the
78 host melanization pathway likely responsible for the formation of the scab phenotype (17).

79 Genome sequencing of the type strain of *F. perrara* and comparison with other genomes of the
80 Orbaceae family revealed the presence of several genomic islands that may be involved in the
81 specific interaction of *F. perrara* with the host (35). These include a biosynthetic gene cluster for
82 the production of the genotoxic metabolite colibactin (Clb), two distinct Type VI Secretion
83 systems (T6SSs), and associated effector proteins, Type I secretion systems, and fimbrial low-
84 molecular-weight protein (Flp) pili genes. However, currently no genetic tools are available for
85 *F. perrara* precluding studies about the role of these genetic factors in gut colonization or the
86 induction of the scab phenotype*.*

87 Here, we report the isolation of a spontaneous mutant of *F. perrara* that possesses a strong
88 colonization defect *in vivo*. Resequencing of the mutant revealed a single nonsynonymous point
89 mutation in the gene encoding the alpha subunit of the DNA-binding protein integration host

90 factor (IHF). Using a combination of gnotobiotic bee experiments, transcriptomics, and
91 metabolite analyses, we characterized the genes regulated by IHF. We then established a gene
92 deletion strategy for *F. perrara,* which allowed us to knockout some of the IHF-regulated genes
93 and show that they impact gut colonization and scab development to different extent.

Results

Isolation of a spontaneous *ihfA* mutant affecting growth and colony morphology of *F. perrara*

Culturing *F. perrara* type strain PEB0191 on modified tryptone yeast glucose (mTYG) agar resulted in the formation of yellow colonies. However, we occasionally observed the appearance of larger white colonies among the yellow ones (**Figure 1A**). Restreaking white colonies on fresh mTYG agar usually resulted in yellow colonies again. However, three white colonies that we identified in independent experiments did not change their appearance anymore, suggesting that we had isolated stable 'white' variants of *F. perrara* PEB0191 (**Figure 1B**). Genome sequencing of the white variants revealed the presence of three different non-synonymous point mutations in the genes encoding the integration host factor (IHF). IHF is a widely distributed DNA-binding protein consisting of the IhfA/B heterocomplex (36-38). Strikingly, two point mutations were identical to each other, but occurred in the different subunits of IHF (*ihfA* and *ihfB*) resulting in a proline to lysine change at amino acid position 82 and 83, respectively (**Figure 1C**). The third point mutation resulted in a lysine to serine change at position 38 of IhfA (**Figure 1C**). Homology modelling showed that these amino acids are located in the region interacting with DNA, suggesting that the three mutations impact the DNA-binding properties of IHF (**Figure 1 D**, (39)). As two of the isolated mutants occurred when generating gene deletion of *F. perrara,* they harbored additional genetic modifications (see Methods). Therefore, we focused further characterization of IHF on the mutation Pro83Lys (hereafter *ihfA**) that occurred in the wild type (wt) background of *F. perrara*. While *IhfA** consistently formed larger colonies than the wt strain on mTYG agar (**Figure 1A and 1B)**, there was no significant difference in growth in liquid culture (Permutation test, $p = 0.097$; **Supplementary Figure 1A**). However, light microscopy showed that cells of the mutant strain were on average slightly longer than cells of the wt (Kolgomorov-Smirnov test $p<0.0001$, **Supplementary Figure 1B and 1C**).

120 ***F. perrara* produces an aryl polyene secondary metabolite that is responsible for the**
121 **yellow colony morphotype.**
122 *F. perrara* PEB0191 encodes a genomic island that is homologous to aryl polyene (APE)
123 biosynthetic gene clusters present in other Gammaproteobacteria (**Figure 2A**). APEs are
124 polyunsaturated carboxylic acids conferring a yellow pigmentation to bacterial cells (40, 41). To
125 assess if *F. perrara* wt, but not the *ihfA** mutant, produces an APE, we cultivated both strains,
126 extracted the pellets, and analyzed the extracts by liquid chromatography coupled to heated
127 electrospray ionization high-resolution mass spectrometry (HPLC-HES-HRMS). The data
128 revealed a strongly UV-Vis-absorbent ion peak at *m/z* 323.1647 $[M+H]^+$, which had a suggested
129 molecular formula of $C_{21}H_{23}O_3$ (**Figure 2B** and **2C**). In the *ihfA** mutant, this ion was only present
130 at trace amounts (**Figure 2C**). To characterize the metabolite in greater detail a larger pellet of
131 *F. perrara* PEB0191 wt cultures was extracted and purified by several HPLC runs. Mass
132 spectrometry- (MS) and UV-Vis-guided fractionation yielded an enriched extract that was
133 analyzed by nuclear magnetic resonance (NMR) spectroscopy. The characteristic ions detected
134 in MS-MS fragmentation experiments (**Supplementary Figure 2**), the UV-Vis spectrum with an
135 absorption maximum at 415 nm (**Supplementary Figure 3**) in conjunction with NMR data
136 (**Supplementary Figure 4-10, Supplementary Table 1**) suggest an aryl polyene structure
137 identical to that reported (42, 43) (**Figure 2D**). Unfortunately it was not possible to connect the
138 NMR substructures because the central methines could not be assigned to chemical shifts
139 (**Figure 2D**, **Supplementary Table 1)**. Comparison of the organic extracts of *F. perrara* wt and
140 *E. coli* CFT073 provided further evidence that both produce the same compound
141 (**Supplementary Figure 11**). Combined, these results suggest that the APE pathway is
142 responsible for the yellow color of the wt colonies of *F. perrara* and is suppressed in the *ihfA**
143 mutant.

144

145 **The *ihfA** mutant of *F. perrara* has a colonization defect and does not cause the scab**
146 **phenotype**
147 As APEs have been shown to increase protection from oxidative stress and contribute to biofilm
148 formation (42, 43), we sought to test if the *ihfA** mutation impacts bee gut colonization. We
149 mono-associated microbiota-free bees with either *F. perrara* wt or *ihfA**. Colonization with the wt
150 strain resulted in a visible scab in 50% and 80% of all bees after five and ten days of
151 colonization, respectively (n=18 and n=36 for both treatments for day 5 and day 10,
152 respectively, **Figure 3A and 3B**). In contrast, none of the bees colonized with the *ihfA** mutant
153 developed a visible scab phenotype. To determine whether this difference was due to a general
154 colonization defect of *ihfA**, we quantified the colonization levels of *F. perrara* at day 5 and day
155 10 post colonization using colony forming units (CFUs). While there was a trend towards lower
156 colonization levels (fewer CFUs and more bees without detectable colonization) for the *ihfA**
157 mutant at day 5 post colonization, the difference was not statistically significant (**Figure 3C**,
158 Wilcoxon rank-sum test p-value=0.076). However, at day 10 post-colonization, bees colonized
159 with the wt strain showed significantly higher CFUs than the *ihfA** mutant (**Figure 3C**, Wilcoxon
160 rank-sum test p-value<0.0001). In fact, in 50% of all bees (n = 36) the colonization levels of
161 *ihfA** were below the detection limit of 500 CFUs (colony forming units) (**Figure 3C**).
162
163 As the quantification of *F. perrara* was based on CFUs obtained for whole-gut tissue, we carried
164 out a second experiment, in which we specifically assessed the colonization levels in the pylorus
165 and the ileum region of the honey bee gut, using both CFUs and quantitative PCR
166 (**Supplementary Figure S12**). The results were comparable to those obtained for the whole
167 gut: at day 10 post colonization, there was a significant difference in the colonization levels of
168 the wt and *ihfA** in both the pylorus and the ileum (Wilcoxon rank-sum test p-value<0.05).
169
170 To obtain a better understanding of the colonization dynamics of *F. perrara* wt and the *ihfA**
171 mutant, we conducted a third gnotobiotic bee experiment in which we inoculated microbiota-free
172 bees with one of the two strains and followed the colonization levels over 12 timepoints from day

173 0 (i.e. 4 h post inoculation) until day 22 post inoculation (**Figure 3D**). We used the same optical
174 density of the two strains for inoculation. However, this corresponded to fewer CFUs for the wt
175 compared to the *ihf** mutant. From the first time point at 4 h post inoculation until day 4 post
176 inoculation, the bacterial levels were below the detection limit (i.e., below 500 CFUs) at both
177 conditions. Between day 4 and day 8 post inoculation, the abundance of *F. perrara* wt increased
178 rapidly to about 10^6 CFUs per gut and then steadily further to 10^7 CFUs per gut until the last
179 timepoint. In contrast, the levels of the *ihfA** mutant remained low until day 10 post colonization
180 and reached on average no more than 10^5 CFUs per gut until the last timepoint at day 22 post
181 colonization. In summary, these results show that *ihfA** has a colonization defect. It has a
182 delayed colonization dynamics as compared to the wt, does not reach the same bacterial loads,
183 and does not cause the scab phenotype.
184

185 **Genes involved in symbiotic interactions are upregulated in *F. perrara* wt relative to the**
186 ***ihfA** mutant**

187 IHF may not have a direct effect on gut colonization, but rather regulate the gene expression of
188 host colonization factors. To test this, we assessed the transcriptional differences by RNA
189 sequencing (RNA-seq) between the wt and *ihfA** mutant when grown *in vitro*. We found that 358
190 out of 2,337 genes encoded in the genome of *F. perrara* PEB0191 were differentially expressed
191 with a log2-fold change >|2| between the two strains (Fisher's exact test with $p<0.05$ and
192 FDR<5%). Of those, 237 and 121 genes were up- and down-regulated in *F. perrara* wt versus
193 *ihfA**, respectively (**Figure 4A and 4B**, **Supplementary Dataset 1**). Among the genes
194 upregulated in the wt, 'Intracellular trafficking, secretion, and vesicular transport' (COG U),
195 'Extracellular structure' (COG W), 'Lipid transport and metabolism' (COG I), 'Mobilome:
196 prophages and transposases' (COG X), and 'Secondary metabolites biosynthesis, transport and
197 catabolism' (COG Q) were significantly enriched (Fisher's exact test, BH-adjusted p-value <
198 0.01; see **Supplementary Dataset 2**). Genes belonging to these three categories include
199 different subunits and effectors of the two T6SSs of *F. perrara*, the Clb biosynthesis gene

200 cluster, various components of the Flp pili, and a RTX (repeats in toxin) toxin belonging to the
201 Type I secretion system family (**Supplementary Dataset 1**). Also, the genes of the APE
202 biosynthesis gene cluster were among the upregulated genes, which is in line with the
203 production of the corresponding metabolites in the wt but not in the mutant strain (**Figure 2**).
204 Interestingly, a relatively large proportion of the upregulated genes encoded hypothetical or
205 poorly characterized proteins. In fact, genes without COG annotation were also enriched relative
206 to the entire genome of *F. perrara* (Fisher's exact test, BH-adjusted p-value < 0.01; see
207 Supplementary **Dataset 2**). Many of the upregulated genes were organized in genomic islands,
208 with the largest one including the biosynthesis gene cluster of Clb and many hypothetical
209 protein-encoding genes (**Figure 4C**). T6SS and Clb biosynthesis genes were among the genes
210 with the highest fold changes relative to *ihfA** mutant (**Figure 4B**, 28 of 32 genes with log2-fold
211 change >6). Moreover, 64% of the upregulated genes (152/237) belonged to the *F. perrara*-
212 specific gene content as based on our previously published genome comparison of *F. perrara*
213 PEB0191 with four other strains of the family Orbaceae (three of the genus *Gilliamella* and one
214 of the genus *Orbus*, **Supplementary Dataset 1)** (35).

215 Among the 121 down-regulated genes, only COG category O ('Posttranslational modification,
216 protein turnover, chaperones') was statistically enriched (Fisher's exact test, BH-adjusted p-
217 value < 0.01, see **Supplementary Dataset 2**). Moreover, only a small fraction (12%) belonged
218 to the "*F. perrara*-specific genes", and fewer genes were organized into genomic islands. A
219 more detailed inspection of the annotation revealed that a large number of the down-regulated
220 genes were involved in transport and metabolism (40 genes), transcriptional regulation (10
221 genes), and protein folding (8 genes), highlighting clear differences in the functional roles of the
222 up- and down-regulated genes. The two genes with the highest fold change (log2-fold change <-
223 5) both encoded transcriptional regulators. One of them, *dksA* (Fpe_01158), is located upstream
224 of the *mrsA*/*mrsB* antioxidant system (Fpe_01159 to Fpe_01162), which was also among the
225 down-regulated genes. The other one is part of the two-component regulator system *basS*/*basR*
226 (Fpe_02097 and Fpe_02098), which has been reported to act as an iron- and zinc-sensing

227 transcriptional repressor and activator in *E. coli* (44, 45). Taken together, these results show that
228 many accessory genes known to be involved in symbiotic interactions (colibactin, Flp pili, T6SS)
229 are upregulated in *F. perrara* wt as opposed to *ihfA**, providing a list of candidate genes
230 responsible for the colonization defect of the *ihfA** mutant.

231

232 **T6SS, pili, APE biosynthesis and Clb biosynthesis genes are expressed during bee gut**
233 **colonization**

234 To test if the genes upregulated *in vitro* in the wt relative to *ihfA** were expressed *in vivo*, we
235 determined the transcriptome of *F. perrara* wt at day 5 and day 10 post colonization. A total of
236 260 (149 up and 111 down) and 298 (162 up and 136 down) genes were differentially
237 expressed at day 5 and day 10 post colonization relative to growth *in vitro* (log2-fold change
238 >|2|, quasi-likelihood F-test with $p<0.05$ and FDR<5%, **Supplementary Dataset 3**). There was a
239 considerable overlap of the genes differentially regulated in vivo relative to in vitro between the
240 two timepoints (115 and 80 shared up- and down-regulated genes, respectively). At both
241 timepoints, the COG category 'Carbohydrate transport and metabolism' (COG G) was
242 significantly enriched among the genes upregulated *in vivo* relative to the entire genome
243 (**Supplementary Dataset 4**). In addition, at timepoint day 10, also the COG category (P)
244 'Inorganic ion transport and metabolism' was enriched (P adj < 0.01, Fisher's exact test,
245 **Supplementary Dataset 4**). Genes belonging to these two categories encoded transporters for
246 different sugars (Phosphotransferase systems), iron, and transferrin (**Supplementary Figure**
247 **13, Supplementary Dataset 3**). In addition, a catalase gene and several genes for the
248 biosynthesis of the amino acid tryptophan were upregulated at both timepoints. However, only
249 14 and 19 genes of the ones upregulated *in vitro* in the wt relative to the *ihfA** mutant (see
250 **Figure 5**), were also upregulated *in vivo* at day 5 and day 10 post-colonization, respectively
251 (**Supplementary Dataset 3**). In fact, several of the T6SS, APE, and Clb biosynthesis genes
252 remained unchanged or were slightly downregulated *in vivo* relative to *in vitro* (**Supplementary**
253 **Dataset 3 and Supplementary Figure 13**). This was not unexpected, because the *in vitro*

254 RNAseq analysis our reference had shown that these genes are already expressed when grown
255 on mTYG agar, which we used as a condition for the *in vivo* analysis. Indeed, when comparing
256 count-normalized gene expression (as measured by TPM) across the different conditions, we
257 found that most of the T6SS machinery, APE biosynthesis, pilus, and iron uptake genes were
258 expressed at similar levels at both timepoints *in vivo* as during *in vitro* growth (**Figure 5,**
259 **Supplementary Figure 14**). Only the Clb genomic island and some of the VgrG-like T6SS
260 effector genes had clearly lower TPM values *in vivo* than *in vitro*, yet higher than in *ihfA** mutant
261 (**Figure 5C and 5F**). These results suggest that most of the genes upregulated in the wt relative
262 to *ihfA* in vitro* were also expressed at high level at both timepoints *in vivo*.
263
264
265 **Gene deletions of IhfA-regulated genes result in impaired gut colonization and/or abolish**
266 **scab development**
267 To test the direct impact of IhfA-regulated genes on host colonization and/or scab development
268 we established a gene deletion strategy for *F. perrara* based on a two-step homologous
269 recombination procedure (see methods). This allowed us to create six different non-polar in-
270 frame gene deletion mutants of potential colonization factors regulated by IHF (Supplementary
271 Table S2). We deleted an essential gene of the colibactin biosynthesis pathway (Δ*clbB*), both
272 *hcp* genes of the two T6SSs, either separately or as double mutant (Δ*hcp1,* Δ*hcp2,* and
273 Δ*hcp1*/Δ*hcp2*), the gene encoding the major Flp pili subunit (Δ*pilE*), and the entire APE
274 biosynthesis gene cluster (Δ*apeA-R*). Deletion mutants were confirmed by genome re-
275 sequencing. The Δ*apeA-R* mutant was the only strain not forming yellow colonies anymore,
276 which is consistent with the idea that the aryl polyene pathway is responsible for the yellow
277 color. To compare the six gene deletion strains to *F. perrara* wt and the *ihfA** mutant in terms of
278 their ability to colonize the honey bee gut and induce the scab phenotype, each strain was
279 inoculated into microbiota-free bees and CFUs assessed in the pylorus/ileum region ten days
280 post inoculation. As expected, *F. perrara* wt successfully colonized the pylorus/ileum region of

281 all analyzed gnotobiotic bees (median = $9.56*10^6 \pm 5.06*10^6$ CFUs per gut; n=18 bees, two
282 independent experiments) and induced the scab phenotype in 16 of 18 bees (**Figure 6**). In
283 contrast, *F. perrara ihfA** colonized poorly compared to the wt (median=$1.46*10^4 \pm 3.19*10^5$
284 CFUs per gut, n= 20 bees, Wilcoxon rank-sum test $P<0.001$), and not a single bee developed
285 the scab phenotype. Of the six tested gene deletion mutants, only the mutant of T6SS-1 (Δ*hcp1*)
286 reached wt colonization levels and also induced the scab phenotype in most of the bees (15 out
287 of 20). The other five mutants all exhibited lower colonization levels than the wt strain. However,
288 the severity of the colonization defect varied between the mutants, and while some of the
289 mutants still caused the scab phenotype, others did not. For example, the Clb biosynthesis gene
290 cluster mutant Δ*clbB* induced the scab phenotype in all but one bee, despite the fact that the
291 colonization levels were about two-fold lower than for the wt (median=$4.24*10^6 \pm 2.87*10^6$ CFUs
292 per gut). The gene deletion mutant of the T6SS-2 (Δ*hcp2*) and the double mutant of both T6SSs
293 (Δ*hcp1*/Δ*hcp2*) reached similar colonization levels as the Δ*clbB* mutant. Yet, none of the bees
294 colonized with these two mutants developed the scab phenotype not even those that had very
295 high bacterial counts (**Figure 6**). The deletion mutant of the APE biosynthesis pathway (Δ*apeA-*
296 *R*) showed again a different colonization phenotype: for some bees no colonization was
297 detected, while others showed similar colonization levels as the wt of *F. perrara*. However, in
298 contrast to the Δ*hcp2* and the Δ*hcp1*/Δ*hcp2* mutants, the Δ*apeA-R* mutant still induced the scab
299 phenotype, but only in the bees that had high bacterial loads. Finally, the Δ*pilE* mutant had the
300 strongest impact on colonization. Only five out of 20 bees had detectable levels of *F. perrara* in
301 the gut (limit of detection: 75 CFUs per gut) and none of the bees developed the scab
302 phenotype. These results confirm that IHF regulates various host colonization factors that when
303 deleted cause distinctive colonization defects.
304

305 **Discussion**

306 In this study, we identified genetic factors that allow the gut symbiont *F. perrara* to colonize its
307 specific niche in the pylorus of the honey bee gut and to induce the scab phenotype. In
308 summary, we found that a nonsynonymous mutation in the gene encoding the alpha subunit of
309 the integration host factor (IhfA) leads to a strong colonization defect of *F. perrara* characterized
310 by reduced bacterial loads in the gut and the absence of the scab phenotype. Using RNAseq,
311 we showed that the *ihfA* mutation (*ihfA**) causes the downregulation of diverse genes known to
312 be involved in symbiosis, including two T6SSs and associated effector proteins, the Clb
313 biosynthetic gene cluster, Flp pili, and an RTX toxin locus. One of the IHF-regulated biosynthetic
314 gene clusters encoded an APE, which we structurally characterized using specialized metabolite
315 analysis, and which seems to be responsible for the yellow appearance of *F. perrara* colonies
316 when grown on mTYG agar. Most of the genes regulated by IhfA were expressed during gut
317 colonization, and gene deletion analysis revealed that the colibactin biosynthesis gene cluster,
318 one of the T6SSs, the Flp pili, and the APE biosynthetic gene cluster impact gut colonization
319 and in part also scab development.

320 These results advance our understanding of the genetic factors that facilitate symbionts to
321 colonize niches in the animal gut. Specifically, we find that the DNA-binding protein IhfA plays
322 an important role in gut colonization. IhfA is a histone-like, nucleoid-associated protein (NAP)
323 that forms a heterodimer together with IhfB. IHF binds to and bends DNA in a sequence specific
324 manner (37-39, 46), thereby facilitating the recombination of mobile DNA elements (37, 38) and
325 influencing gene expression. We identified three different mutations in IHF, all located in the
326 region of the protein interacting with the DNA. All three IHF mutants formed larger colonies than
327 the wt strain on mTYG agar. Together, this suggests that the identified mutations change the
328 DNA-binding properties of IHF resulting in broad transcriptional changes in *F. perrara* that
329 provide a growth advantage in vitro relative to the wt strain.

330 Like other microbiota members inhabiting the pylorus/ileum region of the honey bee gut
331 (*Gilliamella* and *S. alvi*), *F. perrara* colonizes the epithelial surface, where it adheres to the

332 cuticular lining and forms a thick biofilm-like layer (34). In case of the human pathogen
333 *Haemophilus influenzae*, IHF has been shown to bind to extracellular DNA, which increases
334 biofilm stability (47). Therefore, it is possible that IHF has a direct impact on gut colonization of
335 *F. perrara* by stabilizing the biofilm formed on the host epithelium of the pylorus/ileum. However,
336 based on our gene expression data and the results of the gene deletion experiments, it seems
337 more likely that IHF influences gut colonization by regulating downstream genes involved in host
338 interaction. Several of the genes regulated by IHF are known to play important roles in the
339 adhesion to surfaces or the formation of biofilms. For example, pili are key factors for adhesion
340 across many bacteria (48-51) and have already been shown in the case of the bee gut symbiont
341 *S. alvi* to be beneficial for gut colonization and biofilm formation (7). Furthermore, several of the
342 deletion mutants of IHF-regulated genes showed colonization defects in our gnotobiotic bee
343 experiments providing further evidence that IHF impacts gut colonization through its effect on
344 gene expression rather than through a direct role in biofilm formation.

345 The pili mutant (Δ*pilE*) had the strongest colonization defect of the tested gene deletion strains,
346 likely because pili mediate the adhesion to the host epithelium, and therefore allow *F. perrara* to
347 persist and replicate in the pylorus/ileum region of the honey bee gut. The deletion mutant of the
348 APE biosynthesis pathway (Δ*apeA-R*) also showed a clear colonization defect. However, while
349 some of the bees inoculated with this mutant had no detectable levels of *F. perrara* in the gut,
350 others reached similar levels as bees colonized with the wt strain and also developed the scab
351 phenotype. Aryl polyenes can protect bacteria from reactive oxygen species (42, 52) which are
352 produced by insects as part of the host immune response in the midgut (53, 54). Our time
353 course experiment revealed that in the first few days of colonization the bacterial numbers of *F.*
354 *perrara* in the gut are much lower than in the initial inoculum (**Figure 2**) suggesting that the
355 bacteria experience a significant population bottleneck at the beginning of the colonization
356 process. It is possible that the Δ*apeA-R* mutant is impaired in its ability to resist reactive oxygen
357 species (or other physicochemical stressors) when passing through the anterior sections of the
358 honey bee gut and therefore reaches its niche in the pylorus in only a fraction of the inoculated

359 bees. However, APEs have also been implicated in other functions such as biofilm formation
360 (52). Therefore, future studies will be needed to elucidate how the APE biosynthetic pathway of
361 *F. perrara* impacts honey bee gut colonization. Given the widespread occurrence of these
362 biosynthetic genes throughout different bacteria, this might help to understand their role in host
363 colonization in a much wider context (43).

364 A somewhat unexpected result of our mutant analysis was that the deletion of one of the
365 essential NRPS/PKS enzymes of the Clb biosynthetic gene cluster did not affect scab
366 development and had only a weak impact on gut colonization (2-fold lower levels than wt).
367 Studies on *E. coli* have shown that the Clb biosynthesis pathway induces DNA damage in
368 eukaryotic cells (55) and contributes to tumorigenesis in the mammalian gut (56, 57). We have
369 previously shown that *F. perrara* also induces DNA damage in eukaryotic cells and that this is
370 dependent on a functional Clb biosynthesis pathway (35). Therefore, we had speculated that the
371 genotoxic activity of colibactin may trigger the local melanization response and the development
372 of the scab phenotype upon colonization with *F. perrara* (17, 34). However, the results
373 presented here show that colibactin is not causing the scab phenotype. Therefore, other specific
374 characteristics of *F. perrara* must explain why this bacterium but no other honeybee gut
375 symbiont is causing the scab phenotype.

376 Our gnotobiotic bee experiments showed that the development of the scab phenotype depends
377 to a large extent on the bacterial loads of *F. perrara* in the gut. Bees that had $<10^6$ bacteria in
378 the gut did not develop visible scab at day 10 post colonization (**Figure 3 and Figure 7**), which
379 suggests that a certain number of bacteria is needed to elicit this characteristic host response.
380 On the contrary, not all bees with high levels of colonization developed a scab phenotype
381 indicating that high loads are necessary but not sufficient to trigger the development of a visible
382 scab phenotype. Specifically, the *Δhcp2* mutant of T6SS-2 and the *Δhcp* double mutant of
383 T6SS-1 and T6SS-2 both reached relatively high colonization levels, yet not a single bee
384 developed the scab phenotype. T6SS are usually involved in interbacterial warfare by injecting
385 toxins into neighboring bacterial cells (58-60). However, there is an increasing number of

386 studies showing that certain T6SS effectors can also target eukaryotic cells and modify diverse
387 eukaryotic processes, including adhesion modification, stimulating internalization, cytoskeletal
388 rearrangements and evasion of host innate immune responses (61). While *F. perrara* is not the
389 only bee gut symbiont harboring T6SS, the effector protein repertoires differ tremendously
390 between different species and even strains of the same species (62). Thus, it is possible that *F.*
391 *perrara* carries effector proteins, which target the host rather than other bacteria eliciting the
392 melanization response and scab phenotype in the bee gut.

393 We did not carry out a genome-wide screen for host colonization factors, and only generated
394 deletion mutants of a few of the IHF-regulated genes. There are probably many other factors
395 that also contribute to gut colonization. For example, our *in vivo* RNA-seq experiment indicated
396 that metabolic genes involved in tryptophan biosynthesis, sugar transport, and iron uptake are
397 upregulated during gut colonization. This is in line with the TnSeq screen performed in *S. alvi,*
398 which revealed that genes of essential amino acid biosynthesis pathways and iron uptake are
399 important colonization factors of the honey bee gut (63). It is however remarkable that *F. perrara*
400 only upregulates the tryptophan biosynthesis pathway, but no other amino acid biosynthesis
401 genes, which suggest a specific demand for the production of this specific amino acid during gut
402 colonization.

403 While our study revealed that IHF is important for regulating host colonization factors in the
404 honey bee gut, it remains to be elucidated whether IHF is a direct regulator of the identified
405 genes. In *Vibrio fluvialis*, IHF binding sites were identified upstream of several T6SS gene
406 clusters, indicating that direct transcriptional regulation of similar genes by IHF exists in other
407 bacteria (64). Alternatively, IHF may act upstream of another regulator that controls the
408 expression of the identified genes. In the plant pathogen *Dickeya zeae,* IHF was suggested to
409 positively regulate different virulence factors through binding to the promoter region of a
410 diguanylate cyclase gene, increasing the production of the secondary messenger c-di-GMP
411 (65). In *F. perrara,* we found that the transcriptional regulators BasR and DksA were
412 substantially downregulated in the wt versus the *ihfA** mutant. Hence, it is possible that at least

413 some of the differentially regulated genes may not be under the direct control of IHF but
414 regulated via BasR or DskA. In the future, chromatin immunoprecipitation sequencing (ChIP-
415 Seq) could be applied to experimentally identify the specific binding sites of IHF in *F. perrara*
416 and to understand how IHF regulates the gene expression of host colonization factors across
417 bacteria.

418 In conclusion, we identified important gut colonization factors of the bee gut symbiont *F. perrara*
419 and show that they are regulated by IHF. The wide occurrence of these genes in host-
420 associated bacteria suggests similar roles in other environments and calls for a more detailed
421 functional characterization. Our approach to create clean gene deletion mutants expands the
422 available genetic toolbox for bee symbionts (33) and will help to dissect the molecular
423 mechanisms of the identified gut colonization factors in this animal model.

424

425 ## Material and methods

426 ### Bacterial cultivation

427 *F. perrara* strains were cultivated on modified tryptone yeast extract glucose (mTYG) medium
428 (0.2% Bacto tryptone, 0.1% Bacto yeast extract, 2.2 mM D-glucose, 3.2 mM L-cysteine, 2.9 mM
429 cellobiose, 5.8 mM vitamin K, 1.4 µM $FeSO_4$, 72.1 µM $CaCl_2$, 0.08 mM MgSO4, 4.8 mM
430 NaHCO3, 1.36 mM NaCl, 1.8 µM Hematine in 0.2 mM Histidine, 1.25% Agar adjusted to pH 7.2
431 with potassium phosphate buffer) or Columbia Blood Agar (CBA) containing 5% defibrinated
432 sheep blood (Oxoid)) and incubated in anaerobic conditions at 35 °C (8% H_2, 20% N_2, 78% CO_2
433 in a Vinyl Anaerobic Chamber, Coy Lab). Fresh bacterial cultures were used for each
434 experiment. To this end, pre-cultures streaked out from glycerol stocks were grown for 48 hours
435 and re-inoculated onto fresh plates for 16-24 hours of growth. For liquid cultures, pre-cultures
436 streaked out from glycerol stocks were grown on TYG or BHIA plates for 48 hours and then
437 inoculated into fresh liquid TYG or BHI. Cultures were incubated at 34 °C in a ThermoMixer C
438 (Eppendorf) at 800 rpm for 16-24 hours of growth. Strains of *F. perrara* used in this study are
439 listed in **Supplementary Table S2**.

440 ### Rearing and experimental colonization of honey bees

441 Microbiota-depleted bees were generated as described by (18). For experimental mono-
442 colonization, bees were starved for 1-3 hours by removal of the sugar water solution. Then,
443 bees were cooled down to 4 °C in a refrigerator or on ice to transfer them (head side first) into
444 1.5 ml microfuge tubes with a hole at the bottom. Tubes with bees were kept at room
445 temperature. For inoculation, each bee was fed 5 µl of *F. perrara* resuspended in sugar
446 water:PBS (1:1 v/v) through the hole at the bottom of the microcentrifuge tube. The bacterial
447 inocula were adjusted to an OD_{600} of 0.01 or 0.1 depending on the experiment. Colonized bees
448 were kept at 30 °C with 70% humidity while having access to sugar water and sterilized bee
449 pollen *ad libitum* until sampling.

450

451 **Tissue dissection and bacterial quantification from colonized honey bees**

452 Bees were anesthetized by exposure to CO_2. The whole gut or desired gut tissue, e.g., pylorus
453 or ileum was dissected using a scalpel. Malpighian tubules were removed from the gut tissue
454 and the presence of a scab was documented using a dissection stereomicroscope (Leica) as
455 described in (14, 17). The tissues were placed into 2 ml screw-cap tubes containing glass beads
456 (0.75-1 mm diameter, Roth) and 500-1000 µl PBS depending on the experiment.
457 Homogenization of the sample was done by bead beating (FastPrep-24 5g MP Biomedicals) for
458 40 seconds at a speed of 7.5 m/s. Serial dilutions (1:10) were performed for each homogenate
459 and plated onto mTYG or BHI agar. Single colonies were counted to determine the total number
460 of bacteria per gut tissue by multiplying with the dilution factor.

461

462 **RNA sequencing of bacterial *in vitro* cultures**

463 Fresh *F. perrara* cultures were prepared on TYG plates, harvested, and directly transferred into
464 a tube containing TRI reagent (Sigma-Aldrich, Merck) and silica beads (0.1 mm diameter, Roth).
465 Samples were immediately snap frozen in liquid nitrogen and stored at -80 °C until RNA
466 extraction. RNA was extracted using a modified TRI reagent protocol. Samples were
467 homogenized by bead beating with a FastPrep instrument with CoolPrep adapter (FastPrep-24
468 5G, cooled with dry ice) for two cycles of 45 seconds at speed of 6 m/s, including a 30 seconds
469 break between each cycle. Samples were kept at room temperature for 5 min, subsequently
470 extracted using chloroform and RNA was precipitated using isopropanol overnight at -20 °C.
471 Precipitated RNA was dissolved in RNase-free water (Gibco) and incubated with DNase (NEB)
472 to degrade remaining DNA. RNA samples were cleaned up using NucleoSpin RNA clean up kit
473 (Machery-Nagel) according to manufacturer's protocol, eluted in RNAse free water and stored at
474 -80 °C until further use. RNA quality was assessed using Nanodrop, Qubit RNA HS kit
475 (ThermoFisher Scientific) and Bioanalyzer instrument (Agilent). High quality RNA samples were
476 sent to Lausanne Genomic Technology Facility (GTF, University of Lausanne) for RNA
477 sequencing. Samples were depleted of 16S rRNA using RiboZero reagent (Illumina) and Truseq

478 stranded-RNA Zero libraries were generated (Illumina) before sequencing on an Illumina
479 HiSeq2500 generating single-end 100 bp reads.

480

481 **RNA sequencing of bacteria during honey bee gut colonization**

482 Microbiota-depleted bees were colonized with freshly grown *F. perrara*. A fraction of the
483 inoculum was directly transferred into 2 ml tube containing TRI reagent (Sigma-Aldrich, Merck)
484 and silica beads (0.1 mm diameter, Roth). These samples were immediately snap-frozen in
485 liquid nitrogen and stored at -80 °C until RNA extraction, which was carried out in the same way
486 as described in the previous section. For the *in vivo* RNA samples, bees were colonized with *F.*
487 *perrara* as described above and sampled at day 5 and day 10 post inoculation. Guts were
488 removed from anesthetized bees, the pylorus and first part of the ileum was dissected, and the
489 presence of the scab was recorded. For each sample, 10 pylori and ileums from bees coming
490 from the same cage were pooled in a 2 ml screw cap tube containing 750 µl of TRIreagent
491 reagent (Sigma-Aldrich, Merck), glass beads (0.75-1 mm diameter, Roth), and silica beads (0.1
492 mm diameter, Roth). Immediately after collection, samples were snap frozen in liquid nitrogen
493 and stored at -80 °C until RNA extraction. RNA was extracted as described in the previous
494 section. At each time point, four biological replicate samples were used for RNA sequencing,
495 i.e., bees for one sample came from independent cages of gnotobiotic bees. The GTF at the
496 University of Lausanne generated the libraries for the sequencing of the *in vivo* RNA samples.
497 Poly-A depletion was performed in order to enrich for bacterial mRNA and Ribo-zero rRNA
498 depletion was performed in order to remove prokaryotic and eukaryotic rRNAs. Then TruSeq
499 stranded mRNA libraries (Illumina) were generated. The eight libraries were sequenced on an
500 Illumina HiSeq 2500 to obtain single-end 125 bp reads. Libraries of the *in vitro* RNA samples
501 were generated as described before. The four libraries corresponding to the *F. perrara* inocula
502 used for colonizing the bees of the four replicates were sequenced on an Illumina MiniSeq at the
503 Department of Fundamental Microbiology (125 bp single-end reads). Two *in vivo* samples

504 (sample identifier D10_3M and D5_1M) sequenced on the HiSeq 2500 at the GTF were
505 included in the MiniSeq run which confirmed that the two runs gave comparable results.

506

507 **Differential gene expression and gene enrichment analysis**

508 Raw FASTQ files provided by the GTF containing all reads and corresponding tags indicating
509 whether they were accepted or filtered out according to the CASAVA 1.82 pipeline (Illumina).
510 Only reads tagged as accepted were kept for further analysis. FASTQC
511 (http://www.bioinformatics.babraham.ac.uk/projects/fastqc/) was used to control the quality of
512 the data, followed by Trimmomatic (Trimmomatic-0.35) to trim adapters. Filtered and trimmed
513 reads were mapped onto the *F. perrara* genome using Bowtie (bowtie2-2.3.2*)*. Mapped reads
514 were quantified using HTseq (Version 0.7.2). Differential gene expression analysis was done
515 with the Bioconductor package EdgeR (66) using R scripts. For the in vitro RNAseq analysis,
516 negative binomial models were fitted to the data and quantile-adjusted conditional maximum
517 likelihood (qCML) common and tagwise dispersion were estimated. The conditional distribution
518 for the sum of counts in a group was used to calculate the significantly differently expressed
519 genes using an Exact test with a false discovery rate <5%. Only genes detected in all samples
520 with at least 1 count per million were used for the analysis. For the in vivo RNAseq analysis, we
521 followed the recommendations specified in the EdgeR user guide for generalized linear models.
522 In short, read counts were normalized by trimmed mean of M-values (67) producing scaling
523 factors used by EdgeR to determine effective library sizes. Then, negative binomial generalized
524 linear models were fitted for each condition and quasi-likelihood F-tests for each defined
525 contrast (i.e., pairwise comparison between conditions) was used to assess the significance of
526 differentially expressed genes. As for the in vitro RNAseq analysis, only genes with mapped
527 reads with at least 1 count per million in all replicates and conditions were used for the analysis.
528 Genes were considered as differentially expressed upon fulfilling the following criteria: (i) log2
529 fold change ≥ 2 (ii) a p-value of <0.05 and (iii) a false discovery rate <5%. Transcripts per million
530 (TPM) were calculated as follows (68):

$$TPM\ of\ a\ gene = \frac{number\ of\ mapped\ reads * read\ length * 10^6}{total\ number\ of\ transcripts\ sampled * gene\ length\ in\ bp}$$

531 Coverage plots in Figure 2A and Figure 4C were generated with bam2wig.pl contained in the
532 Bio-ToolBox-1.68 (https://github.com/tjparnell/biotoolbox) and visualized with the Integrated
533 Genome Browser (69). Scripts for analyzing the RNAseq data can be found under the following
534 Switchdrive link: https://drive.switch.ch/index.php/s/kCNTp4g7n60ffMi.
535

536 **DNA extraction of dissected gut tissue homogenates**

537 DNA/RNA extraction was performed using an adapted hot phenol protocol from (18) consisting
538 of sample thawing on ice, homogenization by bead beating at 7.5 m/s for 40 seconds (FastPrep-
539 24 5g MP Biomedicals), two phenol extractions, and an ethanol precipitation overnight at -80 °C.
540 DNA/RNA mixture was pelleted and eluted in RNase free water (Gibco). Samples were treated
541 with RNaseA and DNA was purified using a Gel and PCR purification kit (Machery-Nagel).

542

543 **Bacterial quantification by qPCR**

544 Bacterial absolute abundances were determined using quantitative PCR (qPCR) assays
545 targeting the 16S rRNA gene of *F. perrara*. Normalization was based on the number of host
546 actin gene copies as described in (18, 70). Primer sequences and other primer characteristics
547 are given in **Supplementary Table S3**. qPCR was conducted on a StepOne Plus instrument
548 (Applied Biosystems) with the following run method: a holding stage consisting of 2 min at 50 °C
549 followed by 2 min at 95 °C, 40 cycles of 15 sec at 95 °C, and 1 min at 65 °C. A melting curve
550 was generated after each run (15 sec at 95 °C, 20 sec at 60 °C and increments of 0.3 °C until
551 reaching 95 °C for 15 sec) and used to assess specificity of PCR products. qPCR reactions
552 were performed in 10 µL reactions in triplicates in 96-well plates, and each reaction consisted of
553 1 µL of DNA, 0.2 µM of forward and reverse primer and 1x SYBR green "Select" master mix
554 (Applied Biosystems). For each target, standard curves were generated for absolute
555 quantification using serial dilutions (from 10^7 to 10 copies) of the target amplicon cloned into the

556 plasmid vector. Absolute abundance of bacteria was calculated by using the standard curve and
557 were normalized by the median actin copy number per condition (to account for differences in
558 gut size) and by the amount of 16s rRNA copies per genome. For the calculation we used the
559 following formula:

560 $$Absolute\ bacterial\ abundance = 10^{\left(\frac{Ct_{target} - Intercept}{Slope}\right)} * dilution\ factor\ \div number\ of\ 16S\ rRNA\ copies \div$$
561 $$(median\ of\ actin\ copies\ per\ condition)$$

562 Here, Ct_{target} is the cycle threshold of the target bacterium and intercept and slope correspond to
563 the values calculated for the standard curve of the target bacterium.

564

565 **Single cell microscopy**

566 *F. perrara* was freshly grown from stock on plate. Subsequently, liquid overnight cultures
567 starting at an OD_{600} 0.1 were inoculated in TYG. Liquid cultures were grown overnight 16-24
568 hours with shaking at 34 °C in a ThermoMixer C (Eppendorf) in anaerobic atmosphere. The
569 OD_{600} was measured and adjusted to 0.1 – 0.01 and cells were distributed onto small agar
570 patches on a microscopy slide (Milan S.A., Menzel-Gläser). Cells were observed under 1000
571 times magnification using a ZEISS imager M1 microscope with phase contrast (PH3)
572 condenser. Pictures were acquired randomly on the slides with VisiView software, 8-bit images
573 were corrected with ImageJ and the contrast was set at min-value of 0 and max-value of 4000.
574 A 10 µM scale bar was added with ImageJ (71). MicrobeJ plugin for ImageJ was used to
575 measure cell size and area using the acquired pictures (72).

576

577 **Isolation and identification of aryl polyene compounds**

578 *F. perrara* was streaked from the -80 °C glycerol stock onto mTYG plates. Plates were placed in
579 an anaerobic tank with a pack of AnaeroGel 3.5 L (AN0035A Thermo Scientific) at 37 °C and
580 incubated. Under aerobic sterile conditions, colonies were picked and 5 mL of mTYG medium
581 were inoculated in a Hungate tube. After purging the liquid for 1 h with gas (83% N_2, 10% CO_2,
582 7% H_2 v/v) bacteria were grown at 37 °C. After one day of growth, *F. perrara* wt and the *ihfA**

583 mutant were individually cultivated in Hungate tubes containing 30 mL mTYG for three days.
584 Pellets were harvested, extracted with dichloromethane and methanol, then extracts were
585 analyzed by HPLC-HESI-HRMS. The data revealed a strongly UV-Vis absorbent ion peak at
586 *m/z* 323.1647 $[M+H]^+$. To enrich this compound, 400 mL of mTYG were inoculated with 1 mL of
587 pre-culture in a Hungate tube and purged as described above. After 5-10 days all but a few mL
588 of medium were harvested and 400 mL of fresh mTYG was added under sterile aerobic
589 conditions, purged with anaerobic gas and incubated at 37 °C. A total of 3 L of mTYG were used
590 to obtain 6.53 g of cells, which were stored at -80 °C. Light exposure was minimized during all
591 following steps of the aryl polyene enrichment procedure. A mixture of 340 mL dichloromethane
592 and 170 mL of methanol was added to *F. perrara* cell pellets. After 2 h stirring at room
593 temperature (RT), the suspension was filtered and 250 mL KOH (0.5 M) were added. After an
594 additional 1 h of stirring at RT the pH was set to 6 using H_2SO_4 (1 M). The organic layer was
595 washed twice with 500 mL water, once with 250 mL brine, dried over Na_2SO_4 and concentrated.
596 The extract was separated by reverse-phase high performance liquid chromatography (RP-
597 HPLC , Phenomenex Luna 5 µm C18, φ 21.2 x 250 mm, 15.0 mL/min, λ=420 nm) with water
598 +0.1% formic acid (solvent A) and MeCN +0.1% formic acid (solvent B). Solvent compositions of
599 5% B for 4 min, a gradient to 95% B for 18 min, 95% B for 9 min and 5% B for 4 min were used.
600 Fractions around 24 min exhibited strong UV absorption at 420 nm and were further purified by
601 RP-HPLC (Phenomenex Luna 5µ Phenyl-Hexyl, φ 10 x 250 mm, 2.0 mL/min, λ=420 nm) with
602 80% B for 5 min and a gradient of 80% B to 100% B for 30 min. Peaks around 17 min were
603 combined, concentrated and analyzed by NMR spectroscopy. HPLC-HESI-HRMS was
604 performed on a Thermo Scientific Q Exactive mass spectrometer coupled to a Dionex Ultimate
605 3000 UPLC system. NMR spectra were recorded on a Bruker Avance III spectrometer equipped
606 with a cold probe at 500 MHz and 600 MHz for ^{1}H NMR and 125 MHz and 150 MHz for ^{13}C
607 NMR at 298 K. Chemical shifts were referenced to the solvent peaks of DMSO-d_6 at δ_H
608 2.50 ppm and δ_C 39.51 ppm.

609

610 **Structural characterization of the aryl polyene**

611 ^{1}H NMR in conjunction with HSQC data suggested approximately 15 methines and aromatic
612 protons, one methoxy group and one methyl group (**Supplementary Figure 3-6**). From the
613 COSY spectrum, four methines of the conjugated double bond system, and two of the aromatic
614 protons could be connected (**Supplementary Figure 7, 8**). HMBC correlations from the methyl
615 group to an aromatic carbon at δ_C 156 ppm placed it in *ortho*-position of a hydroxy group and
616 next to a singlet aromatic proton. The singlet of the methoxy-group was connected to a carbonyl
617 group by HMBC correlations (**Supplementary Figure 9**).

618

619 **Statistical analysis**

620 Statistical analysis was performed using GraphPad Prism v6.01 or R. Results of all statistical
621 tests can be found in **Supplementary Dataset 5**. Normality was analyzed using D'Agostino-
622 Pearson and/or Shapiro-Wilk test. For comparison with two conditions, t-test was used for
623 parametric data and Wilcoxon sum-rank test or Kolgomorov-Smirnov test for non-parametric
624 data. For comparison of the growth curves of *F. perrara* wt and *ihfA**, we used a permutation
625 test 'compareGrowthCruves' included in the statmod package of R (73).

626

627 **Construction of gene deletion mutants**

628 Targeted in-frame gene deletions of *F. perrara* were constructed using a two-step homologous
629 recombination procedure (see **Supplementary Figure 14**). In a first step, suicide plasmids were
630 constructed harboring two adjacent 700-800 bp-long homology regions matching the up- and
631 downstream region of the gene or gene cluster to be deleted. To this end, the two homology
632 regions were amplified using 2 Phanta Max Master Mix (Vazyme) and cloned into pKS2 using
633 Golden Gate assembly. pKS2 is a derivative of pSEVA312 (74) which contains a sfGFP
634 expression cassette flanked by two BsaI restriction sites in the multiple cloning site. All clonings
635 were done in *E. coli* DH5a/λpir. To validate successful cloning of the two homology regions,

636 PCR and Sanger sequencing was performed. The plasmids derived from pKS2 containing the
637 homology regions were shuttled into the diaminopimelic acid (DAP)-auxotroph *E. coli* JKE201
638 and delivered to *F. perrara* wt via conjugation using bi-parental mating. To this end, *E. coli*
639 JKE201 carrying the plasmid of interest was cultivated for 16-20 hours at 37 °C in LB with
640 500µM DAP (Sigma, LB-DAP) and 30 µg/ml Chloramphenicol. Sub-cultures were made by
641 diluting the culture at a ratio of 1:20 into fresh medium and incubated until exponential growth
642 was reached. A fresh culture of *F. perrara* was prepared by growing it for 36 h on mTYG agar.
643 *F. perrara* and *E. coli* were harvested in PBS and the OD_{600} adjusted to 10. Equal quantities of
644 both bacteria were mixed and spotted onto a cellulose acetate membrane filter (0.2 µm, 25 mm,
645 Huberlab, Sartorius) placed on BHI agar with 500 µM DAP, followed by incubation at 35 °C for 6
646 hours under microaerophilic condition. Filters with bacterial mixtures were removed from the
647 plates with a forceps, placed into a tube with PBS. Bacteria were removed from the filter by
648 pipetting, vortexing and agitation for 10 min at 1500 rpm (Thermomixer C, Eppendorf). The
649 bacterial suspension was centrifuged at 8000x g for 10 minutes, the supernatant discarded to
650 remove dead bacteria and the bacterial pellet was washed once with 1000 µl PBS before
651 resuspending in a reduced volume, i.e. 100 µl PBS. The bacterial mixture was plated onto CBA
652 and TYG with selection antibiotic and incubated at 35 °C for 5 days under anaerobic condition.
653 Colonies were picked after 4-5 days of incubation and expanded to fresh plates. DNA was
654 isolated and five different PCRs performed to check for successful integration of the plasmid into
655 the chromosomal region of *F. perrara* targeted for deletion. Positive clones (loop-in strains) were
656 stocked in liquid mTYG containing 20% (v/v) glycerol at -80 °C until further usage. To select for
657 bacteria that have lost the integrated plasmid, *F. perrara* loop-in strains were grown on mTYG
658 agar and subsequently transformed with plasmid pYE1. pYE1 is a derivative of pBZ485 (75)
659 containing the restriction enzyme *I-SceI* under the control of the IPTG-inducible *lac* promoter.
660 The activity of the restriction enzyme *I-SceI* will negatively select bacteria containing pKS2-
661 derivatives as two *I-SceI* sites are flanking the multiple cloning sites on pKS2. To generate
662 electrocompetent *F. perrara* cells, the bacteria were cultivated from glycerol stocks on mTYG
663 agar and incubated at 35 °C for 2 days under anaerobic condition. Bacteria from plate were

664 inoculated in BHI broth with a starting OD_{600} of 0.1 and grown anaerobically at 40 °C for 12-16
665 hours. Subsequently, growth was stopped by placing cultures onto ice for 15 minutes. Cells
666 were made electrocompetent by washing twice with ice-cold MOPS solution supplemented with
667 20% glycerol, with decreasing volumes per wash. Electrocompetent cells were mixed with >500
668 ng plasmid DNA and incubated for 15 minutes on ice before transferring into an electroporation
669 cuvette. Electroporation was performed applying a voltage of 2.5 kV with resistance of 200 Ω
670 and capacitance of 25 µF. Bacteria were immediately resuspended in BHI and incubated
671 anaerobically for 6 hours at 35 °C to allow phenotypic expression. Bacteria were plated on CBA,
672 mTYG and/or BHIA plates with 25 µg/ml Kanamycin and 100 µM IPTG to select for pYE1 and
673 induce the restriction enzyme *I-SceI*. Plates were incubated in anaerobic atmosphere at 35 °C.
674 After 3 to 5 days of incubation, bacterial colonies were replica plated onto fresh plates
675 containing 15 µg/ml chloramphenicol (selection marker of pKS2-derivatives) or 25 µg/ml
676 kanamycin (selection marker of pYE1) to identify clones that cannot grow on chloramphenicol
677 anymore as a consequence of the loss of the integrated pKS2-derivative. DNA was extracted
678 and a PCR screen performed with primers amplifying the gene targeted for deletion as well as
679 the overspanning region of the deletion. All clones possessing the gene deletion were
680 subsequently expanded on mTYG agar, stocked in glycerol as described above, and subjected
681 to Illumina genome resequencing at Novogene (2x150bp). Mutations in the re-sequenced
682 genomes relative to the genome of the wt strain of *F. perrara* were analyzed with *breseq* (76).

683

684 **Data availability**

685 RNA sequence datasets are available under NCBI Gene Expression Omnibus ID GSE189728.
686 Code, scripts and numeric data files of experimental data have been deposited on Switchdrive:
687 https://drive.switch.ch/index.php/s/kCNTp4g7n60ffMi.

688

689 **Acknowledgments**

690 We thank Stephan Gruber for input regarding the characterization of the ihfA* mutant strain and
691 general feedback for the manuscript. We are grateful to Nicolas Neuschwander and Lucie
692 Kesner for helping with some of the bee experiments. This project was funded by the ERC-StG
693 'MicroBeeOme' (grant agreement No. 714804), the Swiss National Science Foundation (grant
694 agreement No. 31003A_160345 and 31003A_179487), the NCCR Microbiomes (all awarded to
695 PE). J.P. acknowledges funding by the European Research Council (ERC) under the European
696 Union's Horizon 2020 Research and Innovation Program (grant agreement No. 742739).
697

698 **Figures**

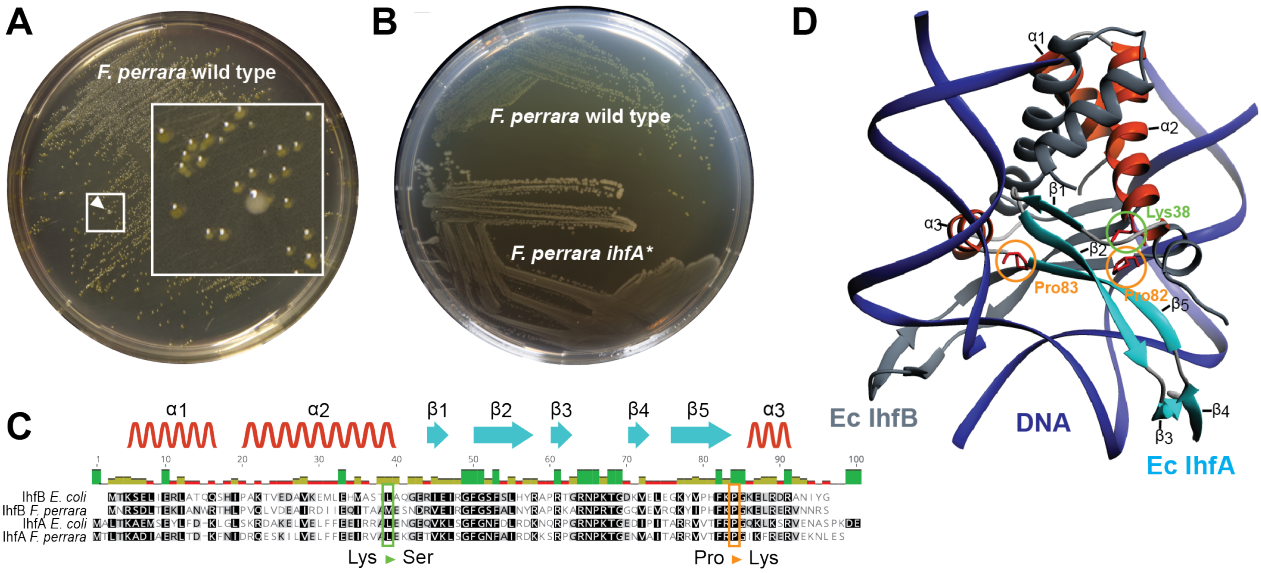

699

700 **Figure 1. Isolation of a spontaneous ihfA* mutant of *F. perrara* displaying an altered**
701 **colony morphotype. (A)** Colonies of *F. perrara* PEB0191 (wt) after 48h of growth on mTYG
702 agar. Arrowhead points at a larger white colony in between many yellow colonies. The area in
703 the white square is magnified. (**B**) Colony morphology of *F. perrara* wt and the isolated white
704 *ihfA** mutant after growth on mTYG for 48h. (**C**) Protein sequence comparison of IhfA and IhfB
705 of *F. perrara* wt and *E. coli*. The mutated lysine and proline residues in IhfA and IhfB are
706 outlined with a green and orange rectangle and the amino acid change due to the point
707 mutations indicated. Secondary structures are depicted above as ribbons (α-helix) and arrows
708 (β-sheet) and are numbered according to their appearance in the protein. (**D**) Three-dimensional
709 structure of *E. coli* IhfA/B heterocomplex with DNA (source protein databank NDB: PDT040).
710 DNA is depicted in blue and IhfB in dark grey. IhfA is colored according to secondary structure:
711 α-helix orange, β-sheet light blue and the rest in light grey. α-helices and β-sheets are
712 numbered. The mutated Pro83 and Lys38 residues of *F. perrara ihfA* and the Pro82 residue of
713 *ihfB* are marked with a orange and green circle, respectively.

714

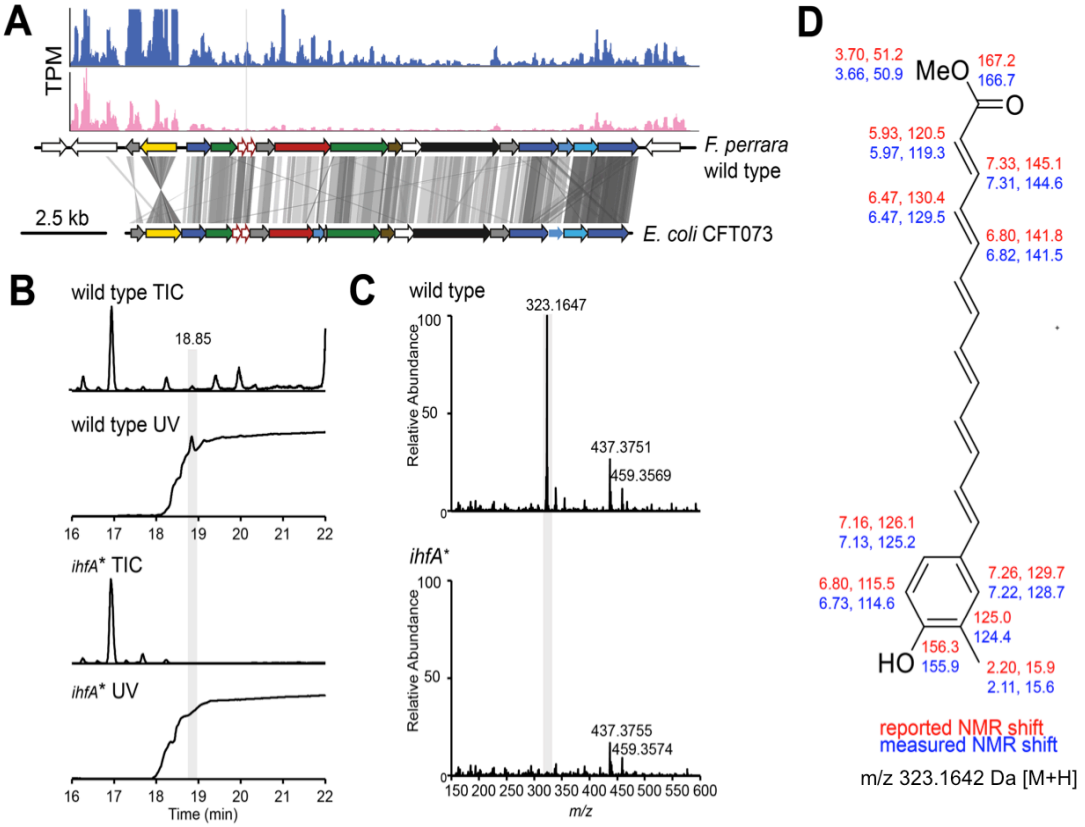

Figure 2. Metabolite analysis of *F. perrara* wt and the *ihfA mutant. (A)** Comparison of gene synteny and sequence similarity of the genomic islands of *F. perrara* PEB0191 (top) and *E. coli* CFT073 (bottom) encoding the aryl polyene (APE) biosynthesis genes. Grey lines indicate homologous regions based on tblastx analysis. Plots were generated with genoplotR (77). Transcripts per million (TPMs) are shown on top of the genomic island for one RNAseq replicate of each *F. perrara* wt (blue) and the *ihfA** mutant grown in vitro. Coverage plots were generated with the Integrated Genome Browser v9 (69). (**B**) Total ion chromatogram (TIC) and UV trace (λ=420 nm) of wt and *ihfA**. A peak highly abundant in the wt was discovered at 18.85 min. Its high UV absorbance at λ=420 nm indicated a conjugated carbon double bond system. (**C**) The normalized mass spectrum at 18.85 min reveals the ion *m/z* = 323.1647 Da to be approximately 50-fold more abundant in the wt compared to *ihfA**. (**D**) Enrichment of the ion containing fraction by HPLC followed by NMR experiments suggest a structure identical to that reported by Cimermancic *et. al.*. Reported (red) and observed (blue) ^{1}H and ^{13}C chemical shifts are shown. Central methenes could not be assigned.

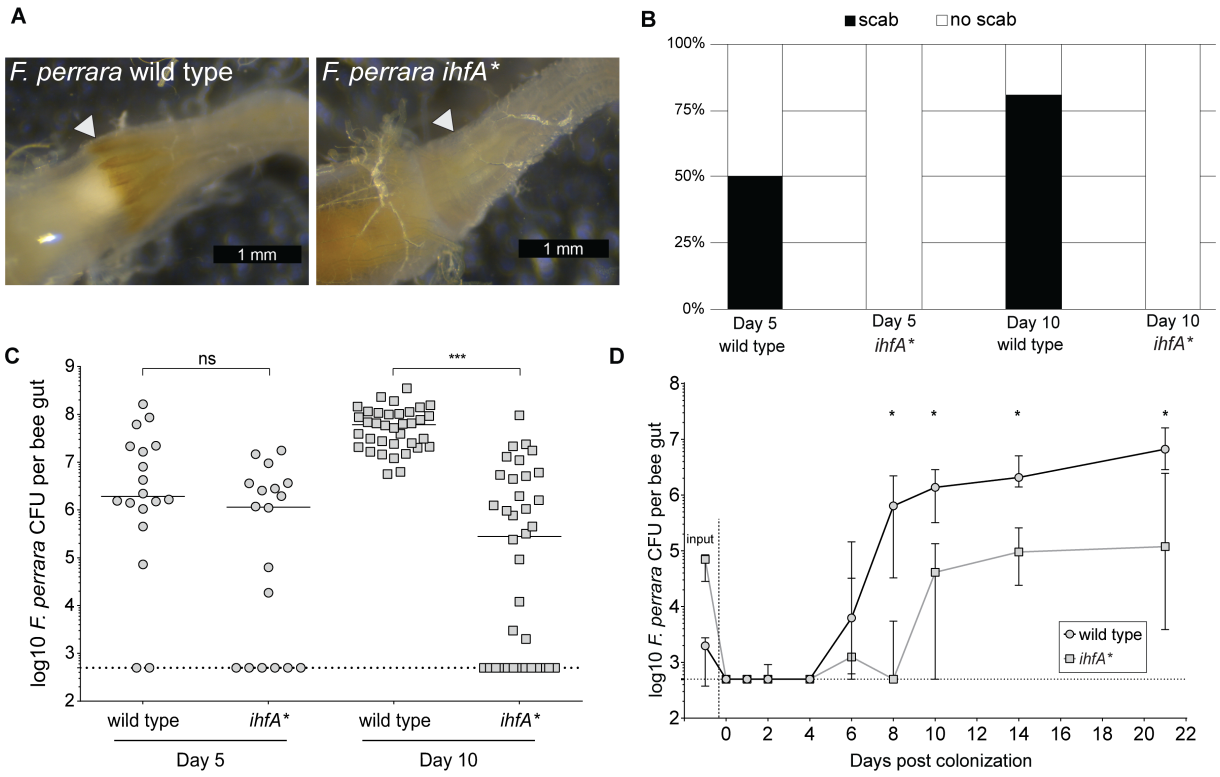

730

731

732 **Figure 3. *F. perrara ihfA** mutant displays a colonization defect. (A)** Light microscopy
733 pictures of pylorus region of bees colonized with *F. perrara* PEB0191wt or *ihfA** 10 days post
734 colonization. (**B)** Quantification of scab phenotype of bees 5 and10 days post colonization with
735 n=18 and n=36 per treatment, respectively. (**C)** Quantification of colonization levels are
736 measured by colony forming units (CFU) 5 (n=18) and 10 (n=36) days post colonization.
737 Wilcoxon rank-sum test was used to assess significant differences. (**D)** Time-course experiment
738 of bees colonized with *F. perrara* wt or *ihfA**. Colonization levels were measured by CFUs every
739 second day until Day 10 and following at Day 14 and Day 21. n=12 per time point per treatment.
740 Wilcoxon rank-sum test was used to assess significant differences per time point. Error bars
741 represent median and interquartile range. Data from three independent experiments. * $p<0.05$,
742 ** $p<0.01$, *** $p<0.001$.

743

744

745

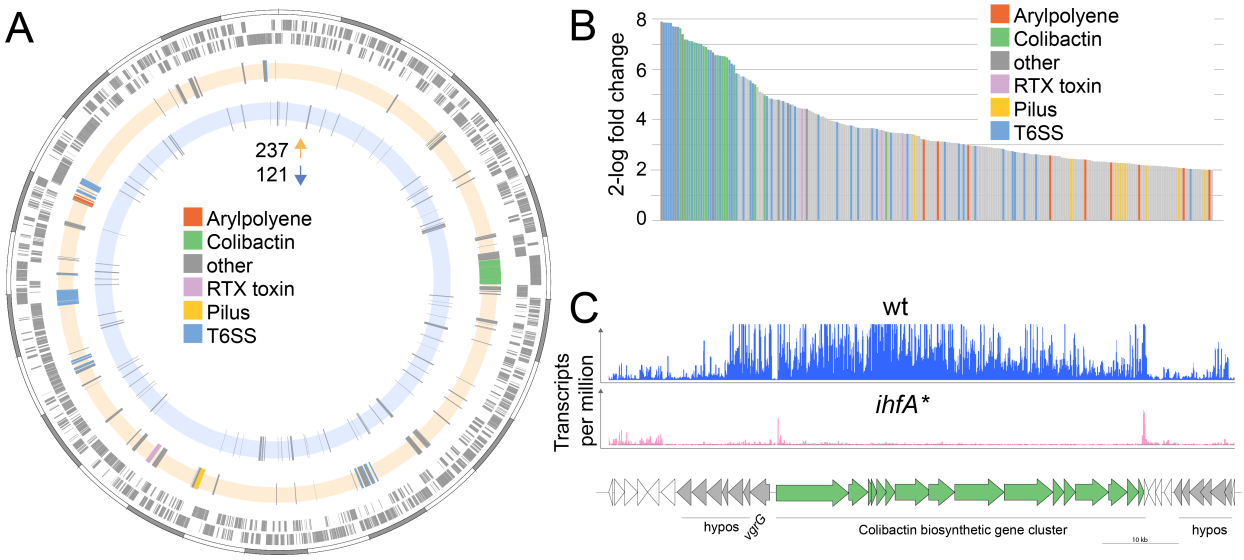

746 **Figure 4. Differential gene expression between *F. perrara* wt and *ihfA** mutant during *in*
747 ***vitro* growth**. (**A)** Chromosomal localization of all genes significantly differentially expressed (2-
748 log fold change = |2|, Fisher's exact test p value <0.05, FDR of <0.05) between *F. perrara* wt
749 and the *ihfA** mutant. Starting from outside, the first circle shows the scale of the genome
750 representation of *F. perrara* in gray and white steps of 100 kb. The second and third circles
751 (gray) depict the genes on the plus and minus strands of *F. perrara*. The fourth (beige) and fifth
752 (light blue) circle depicts genes upregulated and downregulated in wt compared to *ihfA**.
753 Genomic islands are highlighted by coloration. (**B)** Bar plot of the genes differentially expressed
754 between *F. perrara* wt and *ihfA** with a log2-fold change >2 (Fisher's exact test p value <0.05,
755 FDR of <0.05). (**C)** Comparison of the transcriptional profile of the genomic location encoding
756 the colibactin biosynthetic gene cluster between *F. perrara* wt and the ihfA* mutant. Transcripts
757 per million were visualized using the Integrative Genome Browser (69). The colibactin operon is
758 schematically depicted below (green arrows).

759

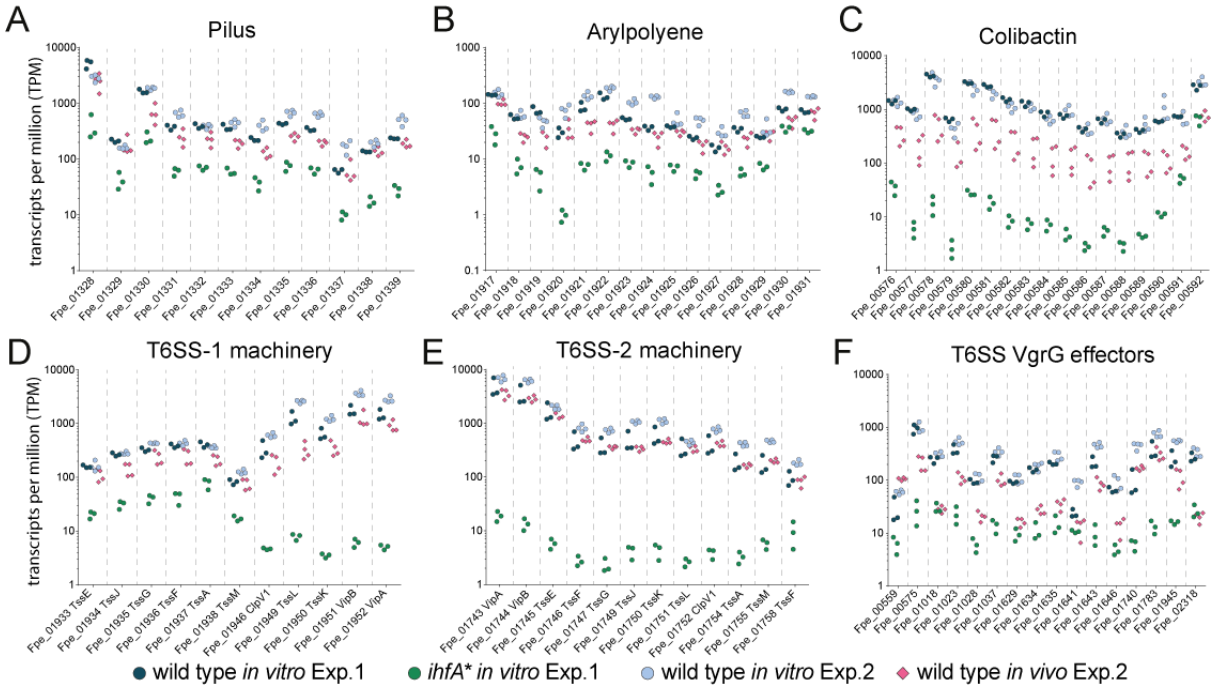

760

761

762 **Figure 5. Gene expression of Ihf-regulated genes of *F. perrara* ten days post-inoculation**
763 **of gnotobiotic honey bees.** Transcripts per million were calculated for all replicates of the *in*
764 *vitro* and the *in vivo* RNAseq experiments. For the in vitro experiment (Exp. 1), all three
765 replicates of the wt and the *ihfA** mutant are shown. For the *in vivo* experiment (Exp. 2), the four
766 replicates of the day 10 time-point and the in vitro reference condition are shown. Data for day 5
767 time-point in comparison to day 10 time-point is shown in **Supplementary Figure14**.

768

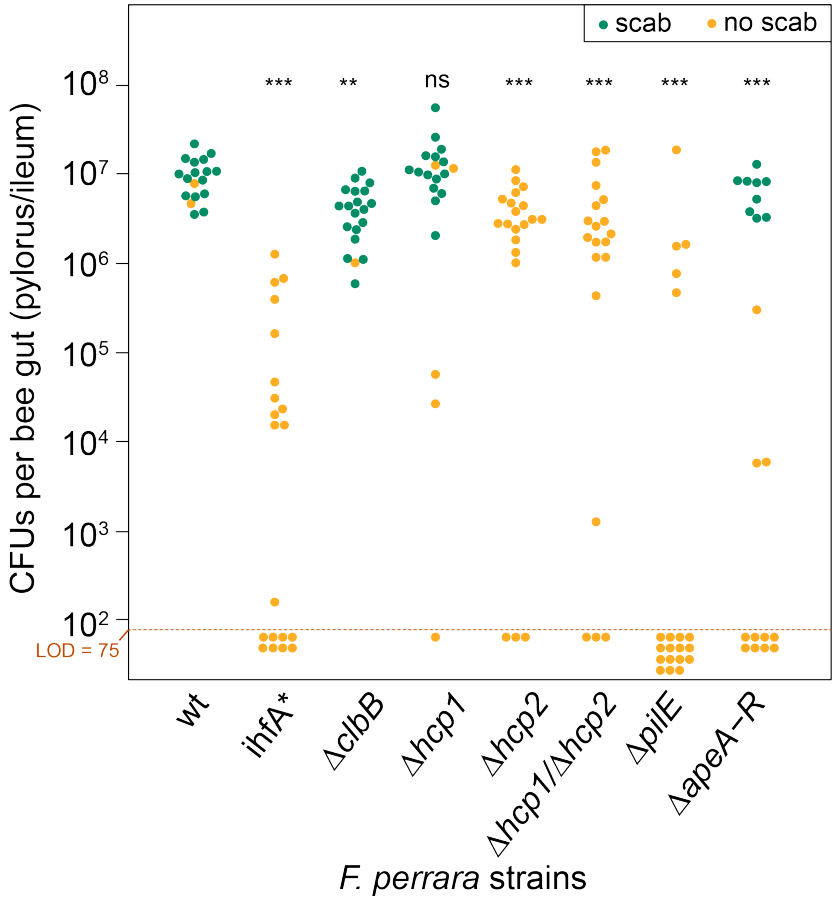

Figure 6. Colonization levels of T6SSs, Clb, Flp pili, and ape gene deletion mutants of *F. perrara.* Colonization levels were assessed 10 days after inoculation by counting colony-forming units (CFU) in dilutions of homogenized bee guts plated on BHI agar. Only the pylorus and ileum section of the gut were analyzed. Limit of detection (LOD) corresponds to the lowest colonization level detectable in our assay, i.e. points below the LOD correspond to bees for which no CFUs were detected. Statistically significant differences of the colonization levels of each mutant relative to the wt of *F. perrara* were determined using the Wilcoxon rank-sum test with BH correction. Bees were inoculated with an OD_{600} of 0.01. Data come from two independent experiments. **Supplementary Figure 15** shows the data points by experiments. * $p<0.05$, ** $p<0.01$, *** $p<0.001$. Filled circle colors indicate whether a scab was detected during dissection (green = scab; yellow = no scab).

785

786 ## Supplementary Figures

787

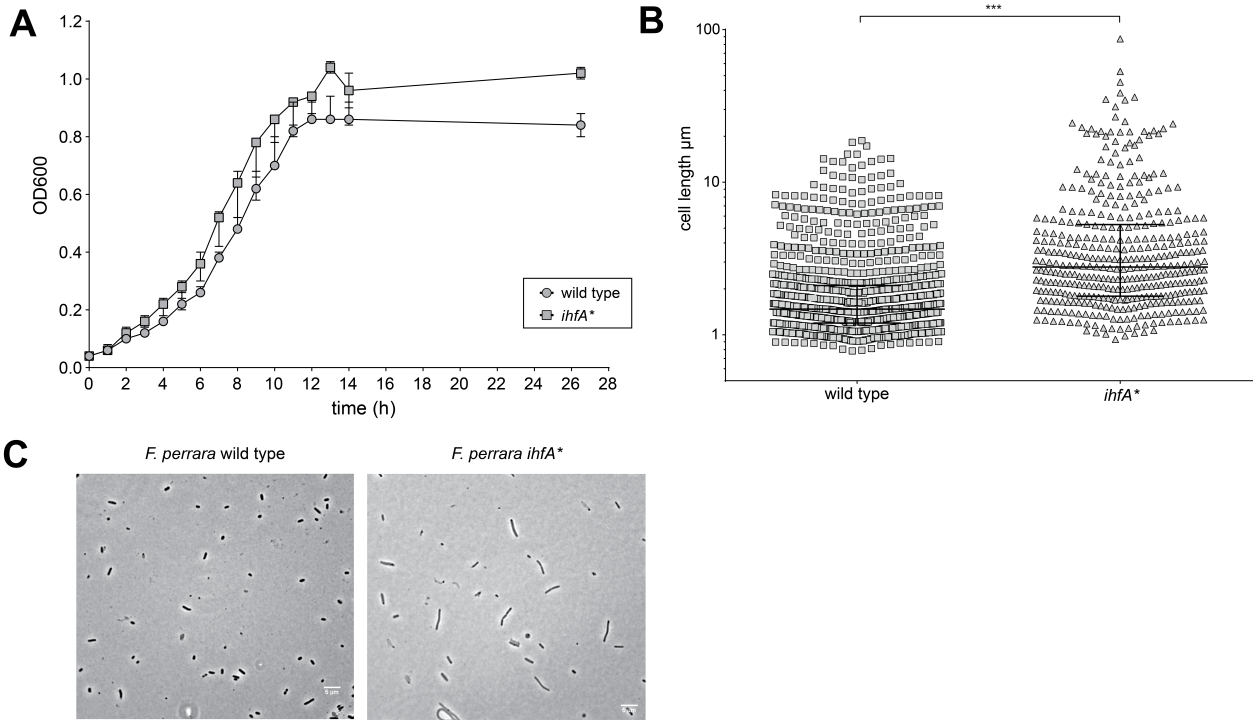

788

789 **Supplementary Figure 1. *In vitro* characterization of *F. perrara ihfA**. (A)** Growth curve of *F.*

790 *perrara* PEB0191 wt and *ihfA** in liquid TYG. The optical density (OD600) was measured every

791 hour for 14 hours (Permutation test, p = 0.097). (**B)** Quantification of single cell length of *F.*

792 *perrara* wt PEB0191 and *ihfA** from the single cell microscopy experiment shown in C.

793 Significance was tested using Kolgomorov-Smirnov test, stars depict significance: *** p<0.0001.

794 **(C)** Single cell light microscopy of *F. perrara* wt and *ihfA**. The scale bar (5µm) is depicted in the

795 right lower corner.

796

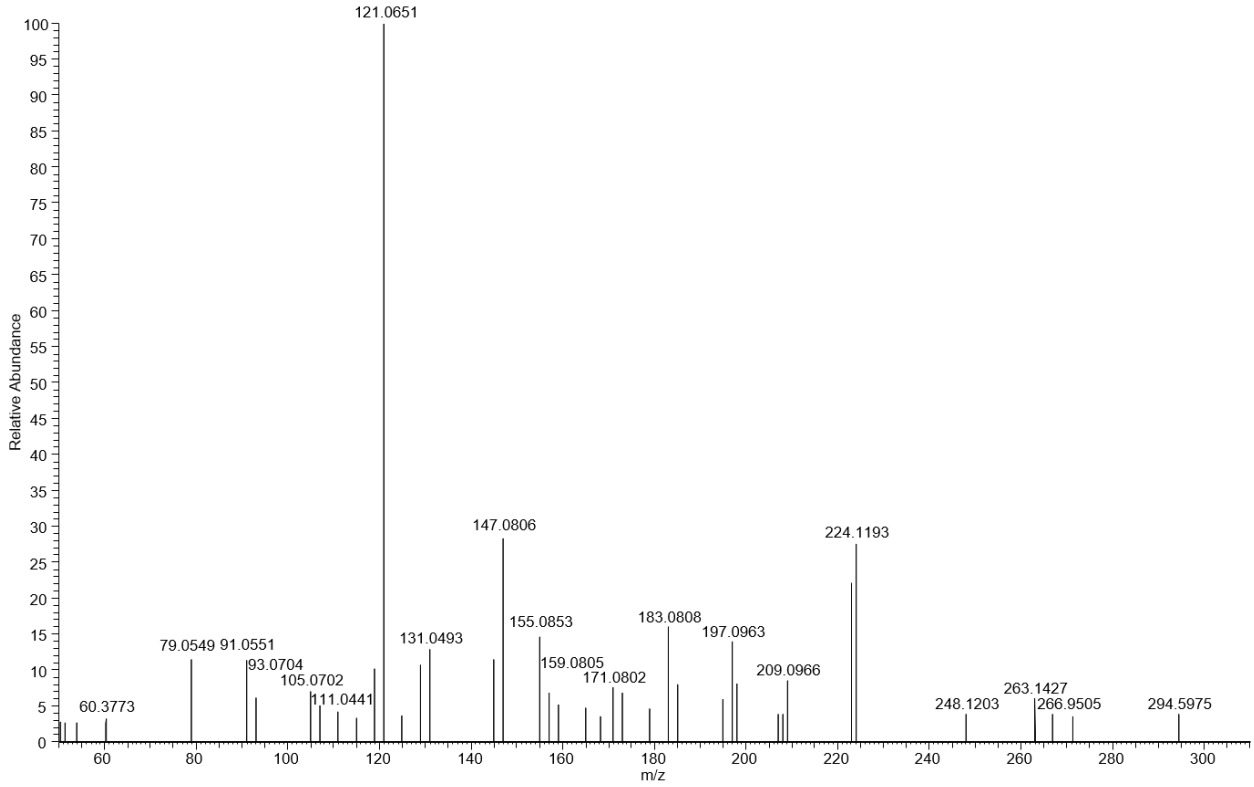

Supplementary Figure 2. Ms-Ms fragmentation spectrum of *m/z* = 323.1647 in extracts of *F. perrara* wt. Many of the prominent ions were reported from aryl polyenes by **(42)**: *m/z*= 121.00, 131.00, 145.00, 147.08, 171.08, 183.00, 197.08, 209.08, 223.08. The spectrum was recorded at 30 kV collision energy.

803

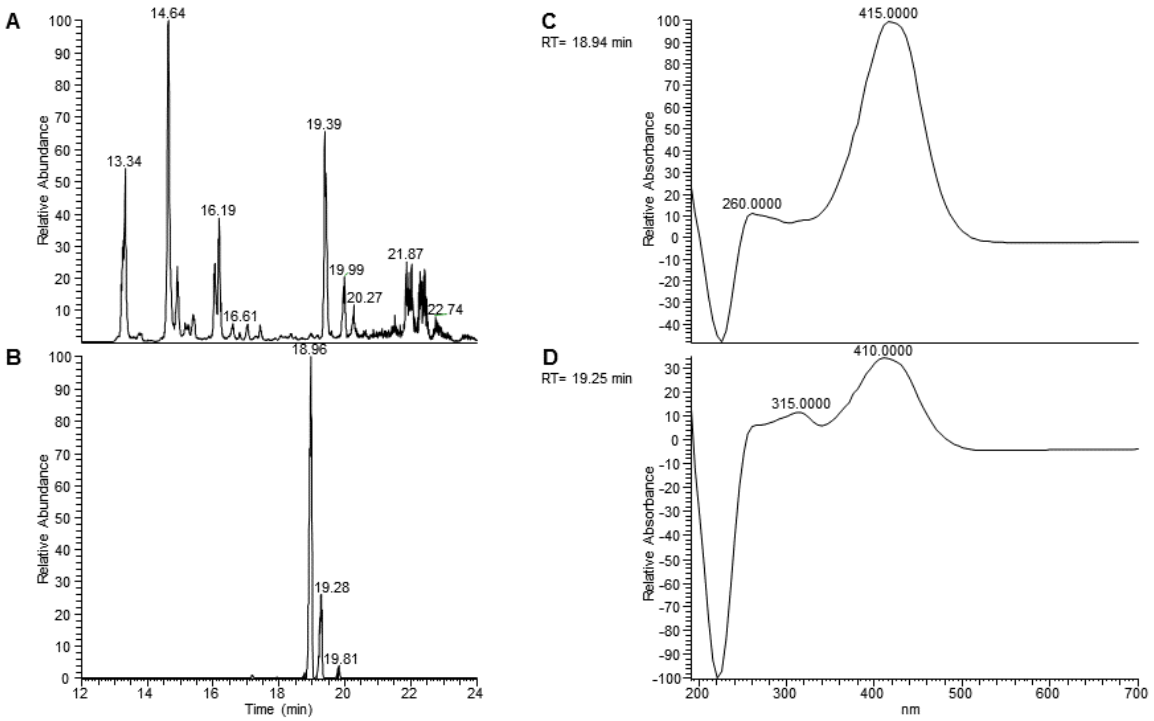

804

805 **Supplementary Figure 3**. **UV-spectrum of the extracts indicates isomerization of the aryl**
806 **polyene.** UV spectrum of the extracts indicates isomerization of the aryl polyene. **A** Total ion
807 chromatogram of extracts of *F*. *perrara* wt. **B** Extracted ion chromatogram of *m/z* = 323.1640 Da
808 (+/- 5ppm). Storage led to the formation of an additional peak at 19.28 min, possibly by
809 isomerization. **C** The UV-spectrum at 18.94 min has the maximum around 415 nm, similar to
810 that reported by (Cimermancic et al., 2014) **D** The UV-spectrum at 19.25 min shows an
811 additional maximum at 315 nm, characteristic for a *trans-cis* conversion of a double bond.

812

813

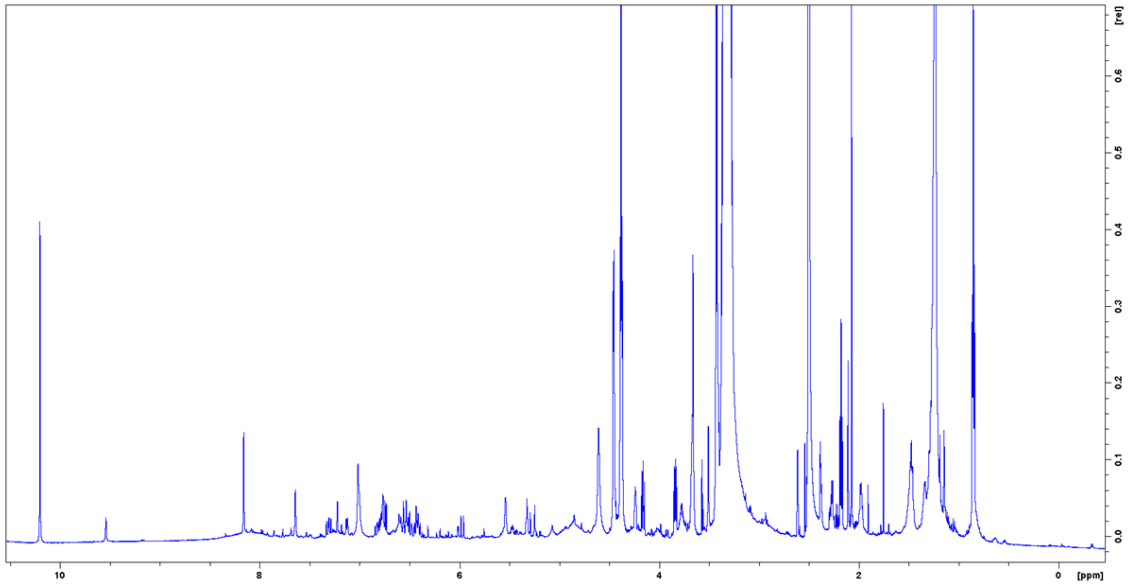

814

815 **Supplementary Figure 4.** ^{1}H NMR spectrum of enriched aryl polyene in DMSO–δ_6 at 298 K.

816

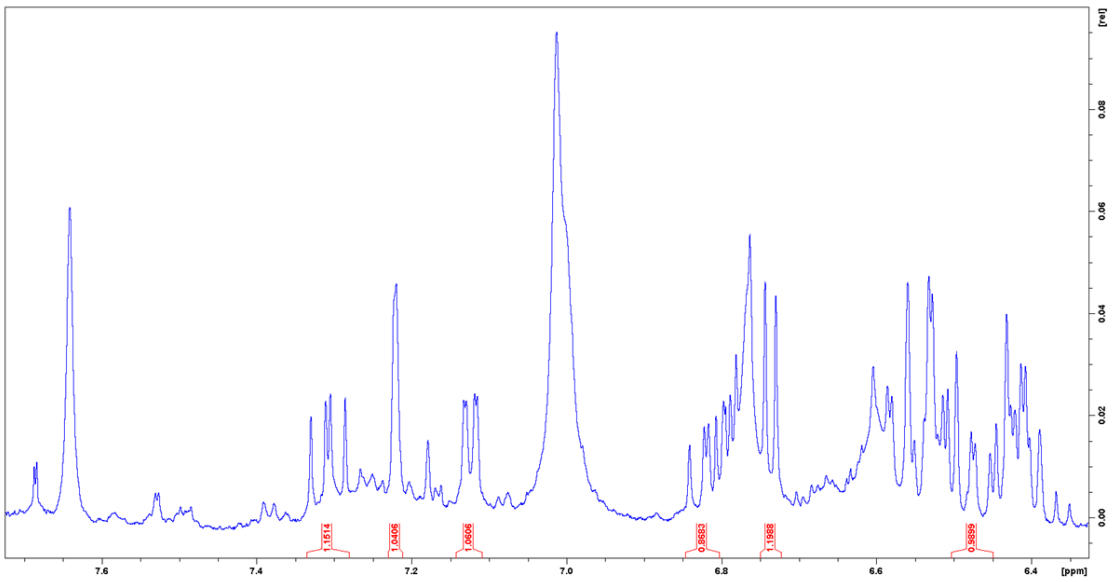

817

818 **Supplementary Figure 5. ^{1}H NMR spectrum of enriched aryl polyene in DMSO–δ_6 at 298 K.**

819 Enhanced view of the aromatic region and integrals of assigned peaks.

820

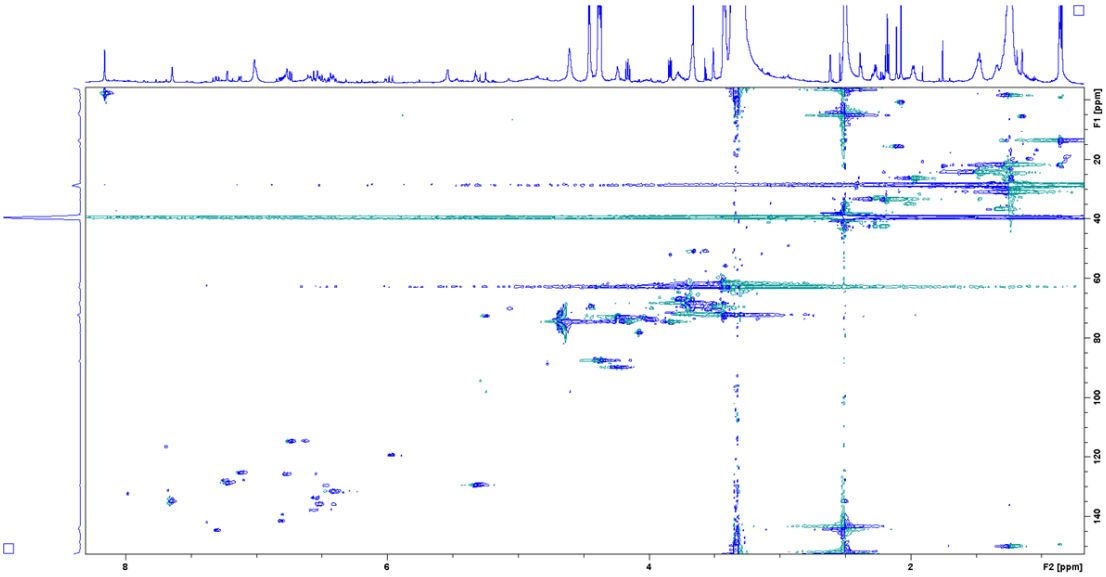

Supplementary Figure 6. HSQC spectrum of enriched aryl polyene in DMSO–δ_6 at 298 K.

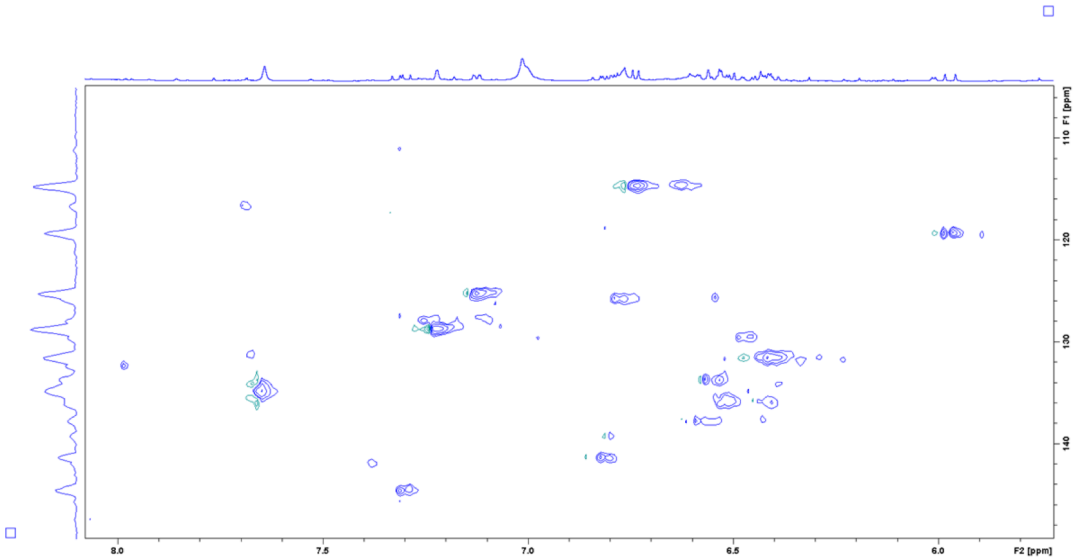

Supplementary Figure 7. HSQC spectrum of enriched aryl polyene in DMSO–δ_6 at 298 K. Enhanced view of the aromatic region.

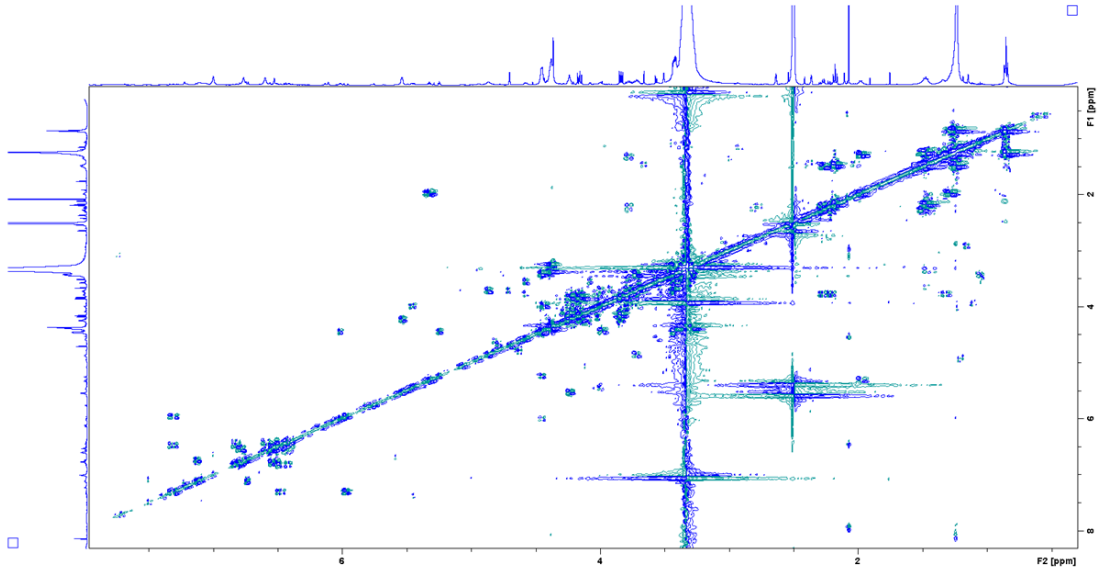

Supplementary Figure 8. COSY spectrum of enriched aryl polyene in DMSO–δ_6 at 298 K.

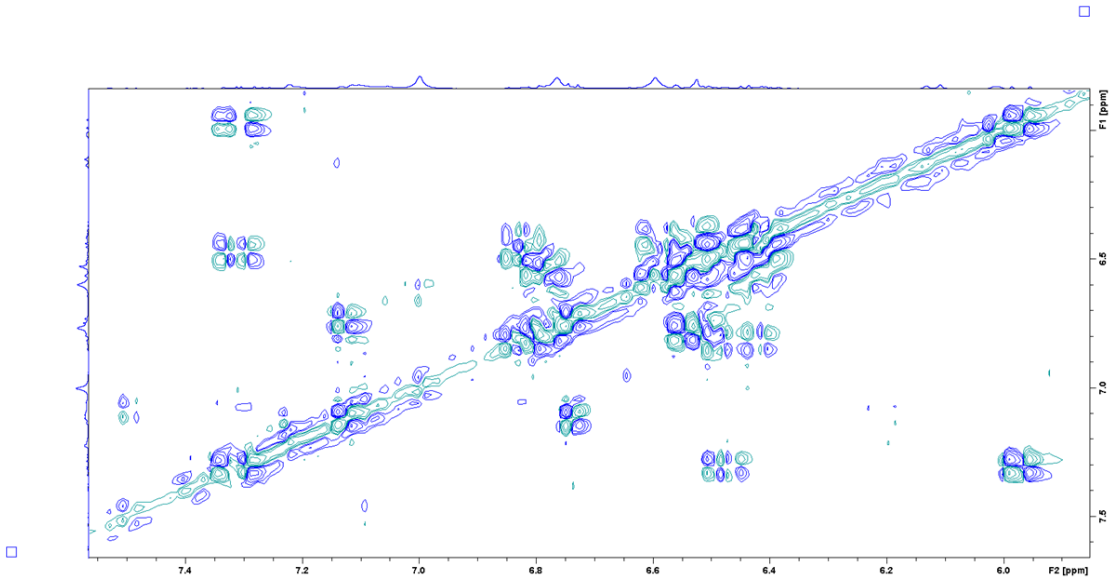

Supplementary Figure 9. COSY spectrum of enriched aryl polyene in DMSO–δ6 at 298 K. Enhanced view of the aromatic region.

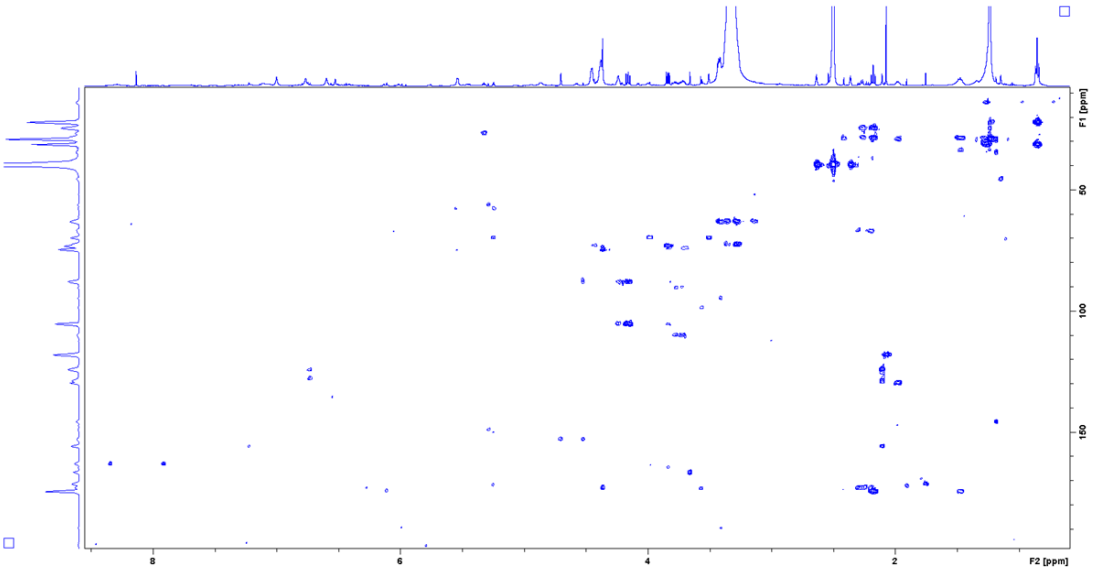

Supplementary Figure 10. HMBC spectrum of enriched aryl polyene in DMSO–δ6 at 298 K.

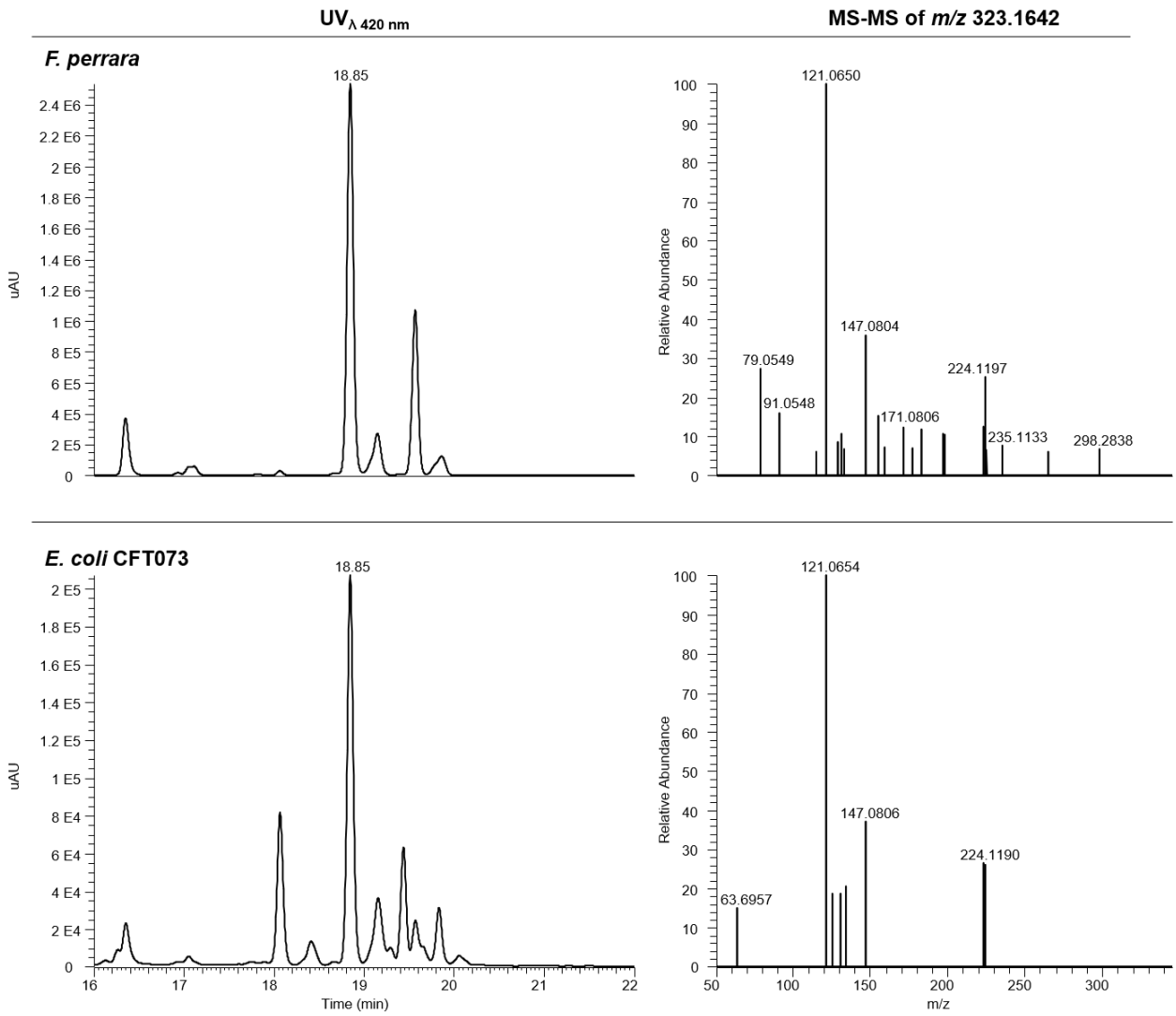

Supplementary Figure 11. HPLC-HRESIMS analysis of *F. perrara* and *E. coli* CFT073. At 18.85 min both extracts show strong absorbance at λ= 420 nm. The MS-MS fragmentation pattern of the ion *m/z* 323.1642 at that retention time shows a similar pattern in extracts from both strains.

844

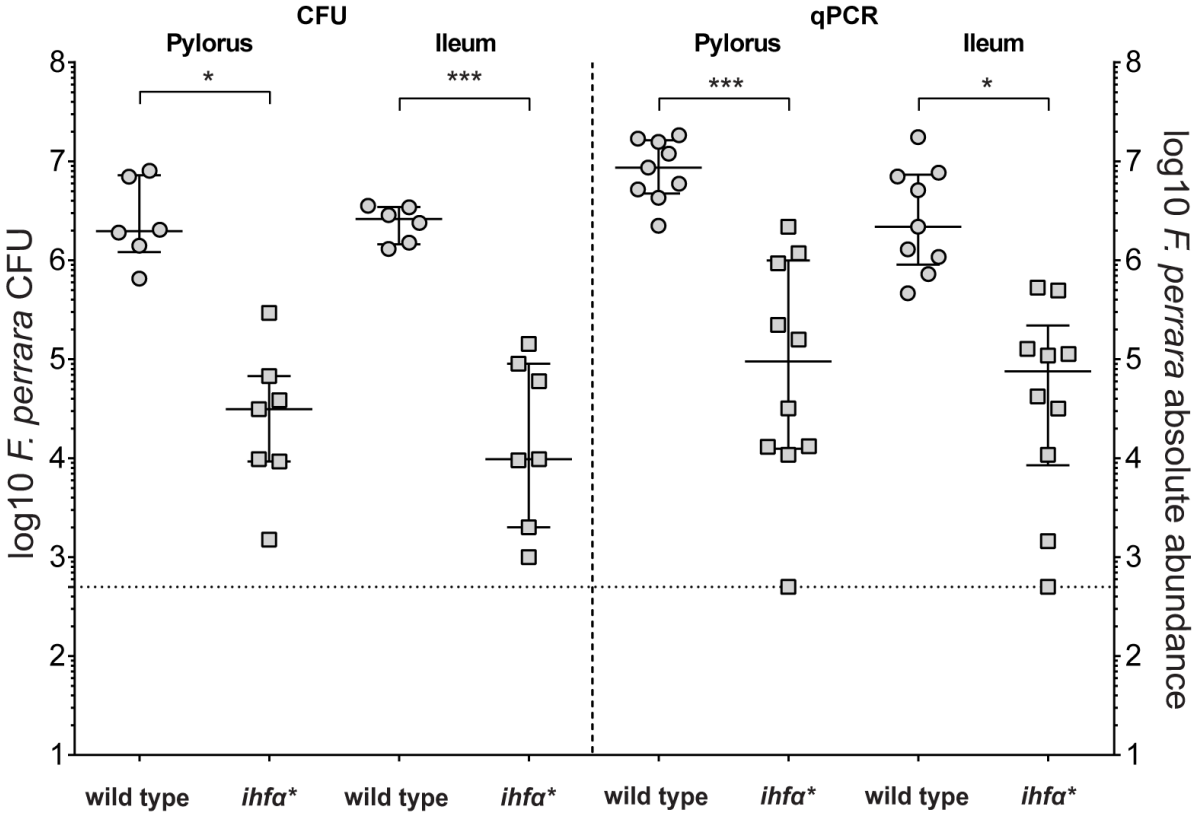

845

846 **Supplementary Figure 12. Quantification of *F. perrara* wt and *ihfA** in pylorus and ileum.**

847 Mono-colonization of bees with *F. perrara* wt and *ihfA**. Colonization levels are measured by

848 colony forming units (CFU) and quantitative PCR (qPCR) 10 days post colonization in the

849 specified gut regions: pylorus and ileum. Wilcoxon rank-sum test was used to assess the

850 statistical significance of differences. n=6.

851

852

853

854

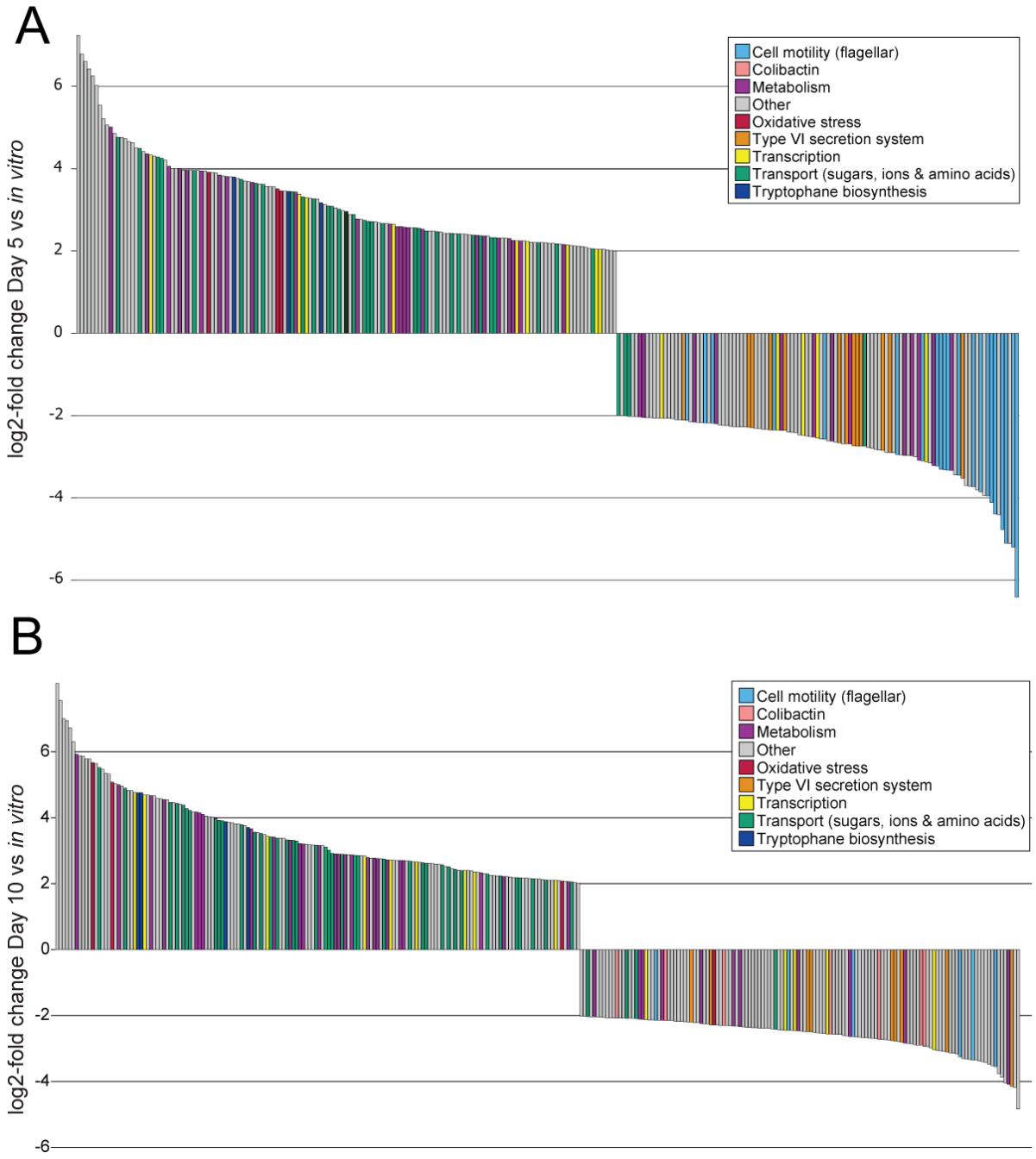

Supplementary Figure 13. RNAseq comparison of *F. perrara* during *in vivo* colonization compared to growth *in vitro*. Significantly differentially expressed genes with a |log2-fold change| >|2| of *F. perrara* PEB0191 wt 5(**A**) and 10 (**B**) days post colonization in comparison to growth *in vitro*. Genes are colored according to their category. The experiment was performed in quadruplicates, all genes displayed were significantly differentially expressed with $p<0.05$ and a FDR of <0.05 (Exact test).

863

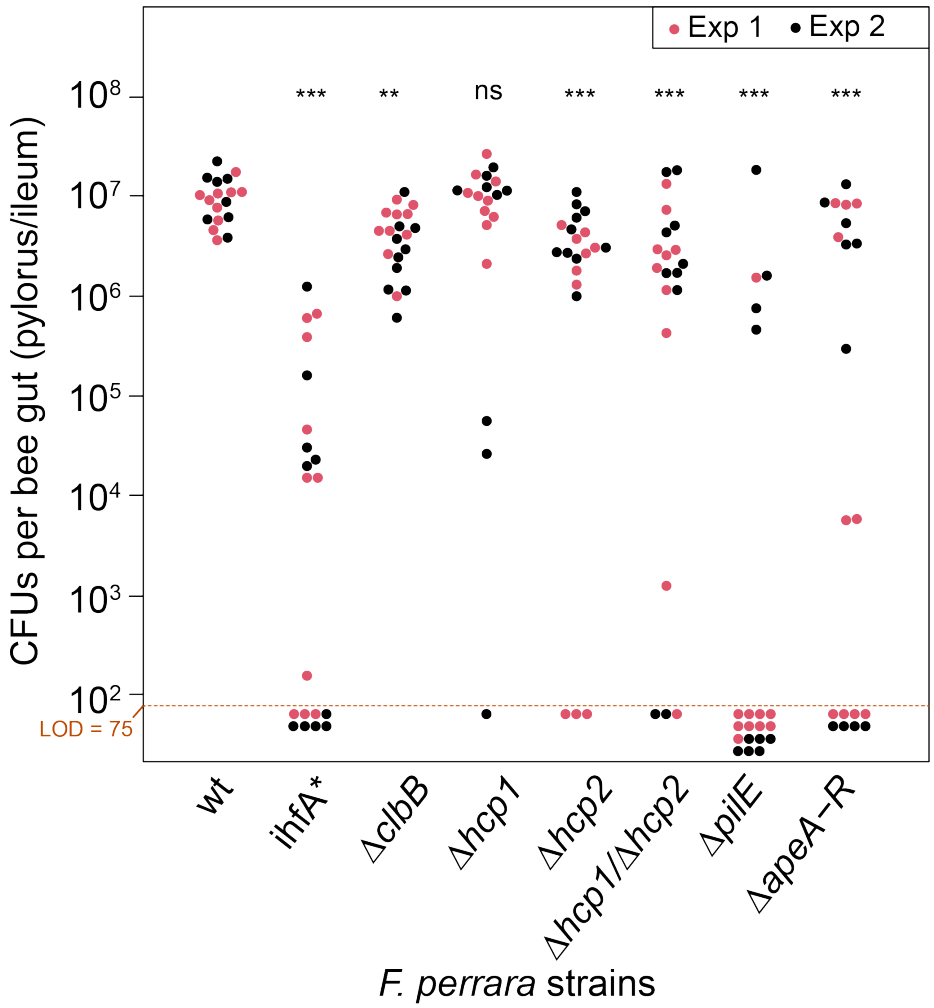

864

865 **Supplementary Figure 14**. Same graph as shown in Figure 7 but datapoints are labelled by

866 experiment.

867

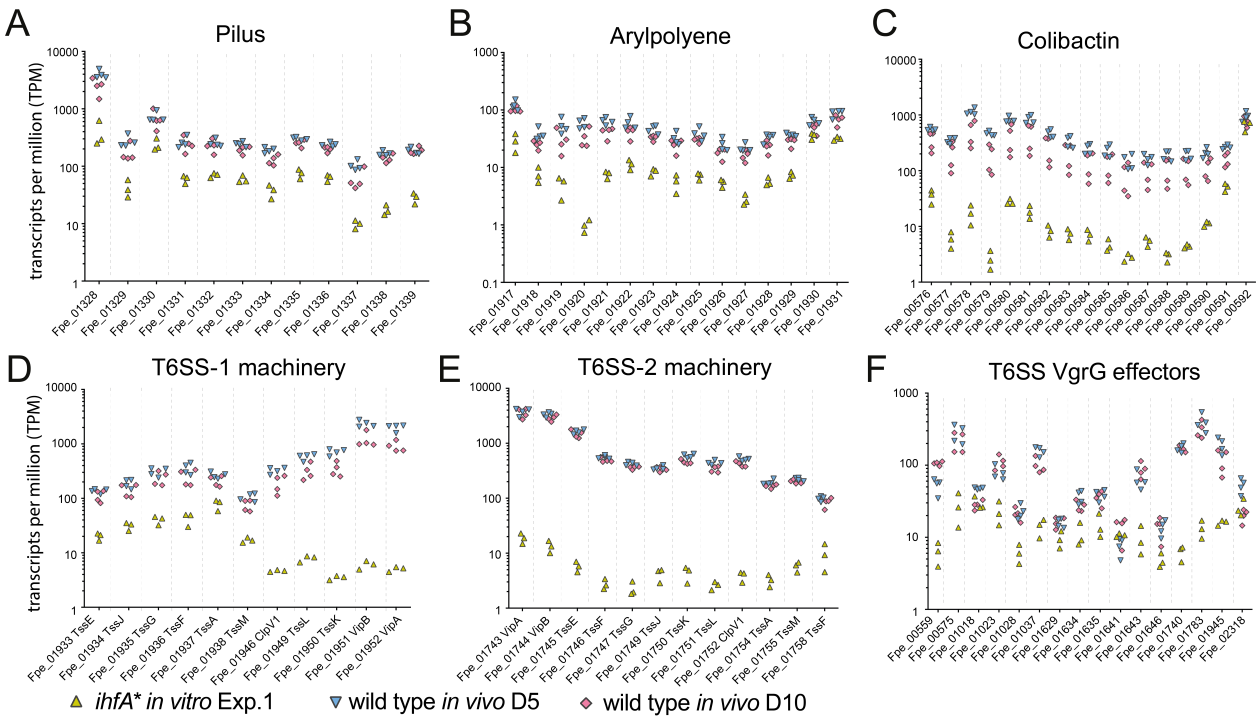

Supplementary Figure 15. **Gene expression of Ihf-regulated genes of *F. perrara* five days post-inoculation of gnotobiotic honey bees**. Same as Figure 5, but only time point Day 5 and Day 10 are depicted in comparison to *F. perrara ihfA* in vitro*.

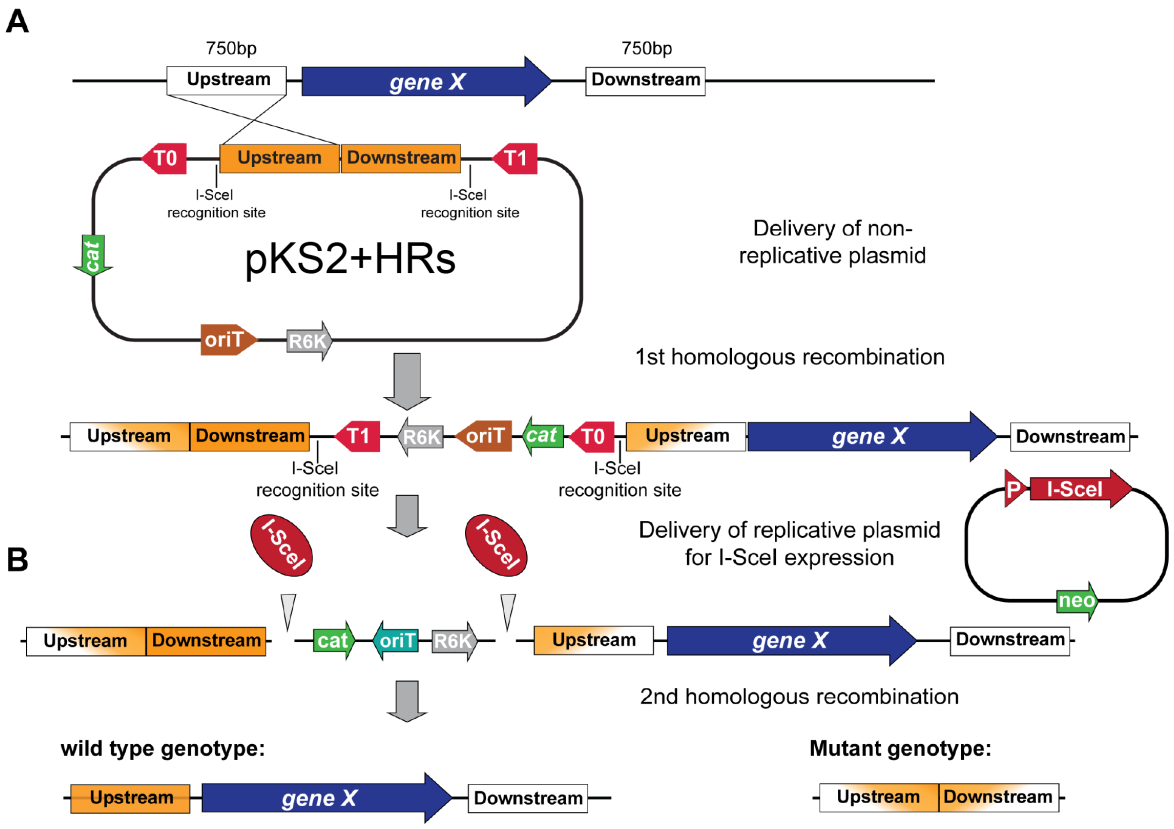

875
876

877 **Supplementary Figure 16. Scheme of the gene deletion strategy based on a two-step**
878 **homologous recombination procedure. A**, A non-replicative plasmid pKS2 integrates via
879 homologous recombination of one of the two cloned 'homology regions' (HRs) upstream or
880 downstream of the gene that is targeted for deletion. **B**, In a second step, a replicative plasmid
881 harboring the restriction enzyme I-SceI is transformed. I-SceI targets corresponding recognition
882 sites located on pKS2 resulting in the selection of either revertant (wt genotypes) or mutant
883 genotypes that underwent a second homologous recombination event in the region targeted for
884 deletion. PCR screening and replica plating on different selective allows to identify to correct
885 clones.
886

887 **Supplementary Tables**

888 **Supplementary Table 1.** Chemical shifts of enriched aryl polyene in DMSO–δ6 at 298 K. Key

889 COSY and HMBC correlation of the enriched polyene.

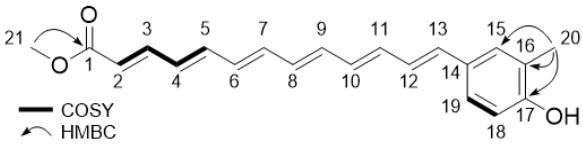

No	δ_C [ppm]	δ_H[ppm], mult.	coupling constant	integral
1	166.7			
2	119.3	5.97, d	*J*=15.1 Hz	0.5
3	144.6	7.33, dd	*J*=11.6 Hz *J*=15.1 Hz	1.2
4	129.5	6.47, dd overlap	*J*=11.6 Hz *J*=14.4 Hz	1.0
5	141.5	6.82, dd overlap	*J*= 11.4 Hz *J*= 14.5 Hz	0.9
6				
7				
8				
9				
10				
11				
12				
13				
14				
15	128.7	7.22, d	*J*=1.7 Hz	1.0
16	124.4			
17	155.9			
18	114.6	6.73, d	*J*=8.3 Hz	1.2
19	125.2	7.13, dd	*J*=1.9 Hz *J*=8.3 Hz	1.1
20	15.6	2.11, s		2.8
21	50.9	3.66, s overlap		3.5

890

891

892 **Supplementary Table 2.** Strains used in this study.

Species	Strain	Genotype*	Mutated gene	Reference	Parent strain
F. perrara	PEB0191/ ESL0157	wild type (wt)	None	(31)	Primary isolate
F. perrara	ESL0158	P83L (CCA→CTA) in *ihfA*	Fpe_00769	This study	PEB0191
F. perrara	ESL0910	P82L (CCA→CTA) in *ihfB;* Δ*apeO*	Fpe_00769; Fpe_01928	This study	PEB0191
F. perrara	ESL0922	L38S (TTA→TCA) in *ihfA;* Δ*pilE**	Fpe_00769; Fpe_00791*; Fpe_01328	This study	PEB0191
F. perrara	ESL0654	Δ*hcp1**	Fpe_01742	This study	PEB0191
F. perrara	ESL0655	Δ*hcp2*	Fpe_01947	This study	PEB0191
F. perrara	ESL0656	Δ*hcp1*, Δ*hcp2*	Fpe_01742, Fpe_01947	This study	PEB0191
F. perrara	ESL0888	Δ*clbB**	Fpe_ 00576	This study	PEB0191
F. perrara	ESL0921	Δ*pilE**	Fpe_01328	This study	PEB0191
F. perrara	ESL0957	Δ*apeA-R**	Fpe_01915-Fpe_01932	This study	PEB0191

*re-sequencing of the genomes revealed that some of the strains (indicated with an asterisk) carried an additional point mutation. However, these mutations were located in random genes and included synonymous as well as non-synonymous base substitutions unlikely to have an effect on the observed phenotypes. The genomic analysis of the re-sequenced strains can be found on the Switchdrive: https://drive.switch.ch/index.php/s/kCNTp4g7n60ffMi.

900 **Supplementary Table 3.** Primers used for qPCR quantification

Primer name	Target	Sequence 5' to 3'	Tm (°C)[a]	Amplicon size (bp)	# Gene loci per genome	Standard curve			
						Primer Efficiency, R^2	Slope, Intercept	LOD Cq[b] (#copies)	Reference
prPEN0013	Actin AB023025 *A. mellifera*	TGCCAACACTGTCCTTTCTG	58.4	156	-	1.896 = 89.6 %, 1.0	-3.6, 37.57	33.7 (10)	(78)
prPEN0014		AGAATTGACCCACCAATCCA	56.4						
prLK-Frisch-042-F	*F. perrara* 16S rRNA gene	GGAAGTTATGTGTGGGATAAGC	60.1	185	4	1.946 = 94.6 %, 0.995	-3.45, 38.04	31.7 (100)	(18)
prLK-Frisch-043-R		CTATTCTCAGGTTGAGCCCG	60.5						

901 a - Melting temperatures were calculated with the online tool described in (Kibbe 2007)

902 b - LOD refers to the limit of detection of primer sets, expressed here as the lowest number of

903 plasmid copies reliably detected by qPCR when standard curves were performed

904

References

1. Wu M*, et al.* (2015) Genetic determinants of in vivo fitness and diet responsiveness in multiple human gut Bacteroides. *Science* 350(6256):aac5992.
2. Lee SM*, et al.* (2013) Bacterial colonization factors control specificity and stability of the gut microbiota. *Nature* 501(7467):426-429.
3. Townsend GE*, et al.* (2019) Dietary sugar silences a colonization factor in a mammalian gut symbiont. *Proceedings of the National Academy of Sciences* 116(1):233-238.
4. Townsend GE*, et al.* (2020) A Master Regulator of Bacteroides thetaiotaomicron Gut Colonization Controls Carbohydrate Utilization and an Alternative Protein Synthesis Factor. *mBio* 11(1):e03221-03219.
5. David LA*, et al.* (2014) Diet rapidly and reproducibly alters the human gut microbiome. *Nature* 505(7484):559-563.
6. Nakajima A*, et al.* (2018) IgA regulates the composition and metabolic function of gut microbiota by promoting symbiosis between bacteria. *Journal of Experimental Medicine* 215(8):2019-2034.
7. Powell JE, Leonard SP, Kwong WK, Engel P, & Moran NA (2016) Genome-wide screen identifies host colonization determinants in a bacterial gut symbiont. *Proceedings of the National Academy of Sciences of the United States of America*.
8. Ohbayashi T*, et al.* (2015) Insect's intestinal organ for symbiont sorting. *Proceedings of the National Academy of Sciences* 112(37):E5179-E5188.
9. Salem H*, et al.* (2017) Drastic Genome Reduction in an Herbivore’s Pectinolytic Symbiont. *Cell* 171(7):1520-1531.e1513.
10. Kikuchi Y, Ohbayashi T, Jang S, & Mergaert P (2020) Burkholderia insecticola triggers midgut closure in the bean bug Riptortus pedestris to prevent secondary bacterial infections of midgut crypts. *The ISME journal*.
11. Kwong WK & Moran NA (2016) Gut microbial communities of social bees. *Nature reviews. Microbiology* 14(6):374-384.
12. Bonilla-Rosso G & Engel P (2018) Functional roles and metabolic niches in the honey bee gut microbiota. *Curr Opin Microbiol* 43:69-76.
13. Kwong WK*, et al.* (2017) Dynamic microbiome evolution in social bees. *Sci Adv* 3(3):e1600513.
14. Engel P, Bartlett KD, & Moran NA (2015) The Bacterium Frischella perrara Causes Scab Formation in the Gut of its Honeybee Host. *mBio* 6(3).
15. Martinson VG*, et al.* (2011) A simple and distinctive microbiota associated with honey bees and bumble bees. *Molecular ecology* 20(3):619-628.
16. Powell JE, Martinson VG, Urban-Mead K, & Moran NA (2014) Routes of Acquisition of the Gut Microbiota of the Honey Bee Apis mellifera. *Appl Environ Microbiol* 80(23):7378-7387.
17. Emery O, Schmidt K, & Engel P (2017) Immune system stimulation by the gut symbiont Frischella perrara in the honey bee (Apis mellifera). *Molecular ecology* 26(9):2576-2590.
18. Kesnerova L*, et al.* (2017) Disentangling metabolic functions of bacteria in the honey bee gut. *bioRxiv*.
19. Raymann K, Bobay LM, & Moran NA (2018) Antibiotics reduce genetic diversity of core species in the honeybee gut microbiome. *Mol Ecol* 27(8):2057-2066.
20. Zheng H, Powell JE, Steele MI, Dietrich C, & Moran NA (2017) Honeybee gut microbiota promotes host weight gain via bacterial metabolism and hormonal signaling. *Proceedings of the National Academy of Sciences of the United States of America* 114(18):4775-4780.

21. Brochet S*, et al.* (2021) Niche partitioning facilitates coexistence of closely related honey bee gut bacteria. *Elife* 10.
22. Ellegaard KM*, et al.* (2019) Genomic changes underlying host specialization in the bee gut symbiont Lactobacillus Firm5. *Molecular ecology* 28(9):2224-2237.
23. Ellegaard KM & Engel P (2019) Genomic diversity landscape of the honey bee gut microbiota. *Nature communications* 10(1):446.
24. Engel P, Martinson VG, & Moran NA (2012) Functional diversity within the simple gut microbiota of the honey bee. *Proceedings of the National Academy of Sciences of the United States of America* 109(27):11002-11007.
25. Kwong WK, Engel P, Koch H, & Moran NA (2014) Genomics and host specialization of honey bee and bumble bee gut symbionts. *Proceedings of the National Academy of Sciences of the United States of America* 111(31):11509-11514.
26. Kwong WK*, et al.* (2017) Dynamic microbiome evolution in social bees. *Science Advances* 3(3).
27. Ludvigsen J, Porcellato D, Amdam GV, & Rudi K (2018) Addressing the diversity of the honeybee gut symbiont Gilliamella: description of Gilliamella apis sp. nov., isolated from the gut of honeybees (Apis mellifera). *Int J Syst Evol Microbiol* 68(5):1762-1770.
28. Steele MI, Kwong WK, Whiteley M, & Moran NA (2017) Diversification of Type VI Secretion System Toxins Reveals Ancient Antagonism among Bee Gut Microbes. *mBio* 8(6).
29. Zheng H*, et al.* (2019) Division of labor in honey bee gut microbiota for plant polysaccharide digestion. *Proceedings of the National Academy of Sciences* 116(51):25909-25916.
30. Volkmann M*, et al.* (2010) Orbus hercynius gen. nov., sp. nov., isolated from faeces of wild boar, is most closely related to members of the orders 'Enterobacteriales' and Pasteurellales. *Int J Syst Evol Microbiol* 60(Pt 11):2601-2605.
31. Engel P, Kwong WK, & Moran NA (2013) Frischella perrara gen. nov., sp. nov., a gammaproteobacterium isolated from the gut of the honeybee, Apis mellifera. *International Journal of Systematic and Evolutionary Microbiology* 63(10):3646-3651.
32. Martinson VG, Moy J, & Moran NA (2012) Establishment of characteristic gut bacteria during development of the honeybee worker. *Appl Environ Microbiol* 78(8):2830-2840.
33. Leonard SP*, et al.* (2018) Genetic Engineering of Bee Gut Microbiome Bacteria with a Toolkit for Modular Assembly of Broad-Host-Range Plasmids. *ACS Synth Biol* 7(5):1279-1290.
34. Engel P, Bartlett KD, & Moran NA (2015) The Bacterium Frischella perrara Causes Scab Formation in the Gut of its Honeybee Host. *MBio* 6(3):e00193-00115.
35. Engel P, Vizcaino MI, & Crawford JM (2015) Gut symbionts from distinct hosts exhibit genotoxic activity via divergent colibactin biosynthesis pathways. *Appl Environ Microbiol* 81(4):1502-1512.
36. Friedman DI (1988) Integration host factor: A protein for all reasons. *Cell* 55(4):545-554.
37. Freundlich M, Ramani N, Mathew E, Sirko A, & Tsui P (1992) The role of integration host factor in gene expression in Escherichia coli. *Molecular microbiology* 6(18):2557-2563.
38. Goosen N & van de Putte P (1995) The regulation of transcription initiation by integration host factor. *Molecular microbiology* 16(1):1-7.
39. Rice PA, Yang S-w, Mizuuchi K, & Nash HA (1996) Crystal Structure of an IHF-DNA Complex: A Protein-Induced DNA U-Turn. *Cell* 87(7):1295-1306.
40. Goel AK, Rajagopal L, Nagesh N, & Sonti RV (2002) Genetic Locus Encoding Functions Involved in Biosynthesis and Outer Membrane Localization of Xanthomonadin in Xanthomonas oryzae pv. oryzae. *J Bacteriol* 184(13):3539-3548.
41. Poplawsky AR, Urban SC, & Chun W (2000) Biological role of xanthomonadin pigments in Xanthomonas campestris pv. campestris. *Appl Environ Microbiol* 66(12):5123-5127.

42. Schoner TA*, et al.* (2016) Aryl Polyenes, a Highly Abundant Class of Bacterial Natural Products, Are Functionally Related to Antioxidative Carotenoids. *Chembiochem* 17(3):247-253.
43. Cimermancic P*, et al.* (2014) Insights into secondary metabolism from a global analysis of prokaryotic biosynthetic gene clusters. *Cell* 158(2):412-421.
44. Lee LJ, Barrett JA, & Poole RK (2005) Genome-wide transcriptional response of chemostat-cultured Escherichia coli to zinc. *J Bacteriol* 187(3):1124-1134.
45. Hantke K (2001) Iron and metal regulation in bacteria. *Current opinion in microbiology* 4(2):172-177.
46. Zulianello L, van Ulsen P, van de Putte P, & Goosen N (1995) Participation of the Flank Regions of the Integration Host Factor Protein in the Specificity and Stability of DNA Binding. *Journal of Biological Chemistry* 270(30):17902-17907.
47. Jurcisek JA, Brockman KL, Novotny LA, Goodman SD, & Bakaletz LO (2017) Nontypeable Haemophilus influenzae releases DNA and DNABII proteins via a T4SS-like complex and ComE of the type IV pilus machinery. *Proc Natl Acad Sci U S A* 114(32):E6632-E6641.
48. Utada AS*, et al.* (2014) Vibrio cholerae use pili and flagella synergistically to effect motility switching and conditional surface attachment. *Nat Commun* 5:4913.
49. Tomich M, Planet PJ, & Figurski DH (2007) The tad locus: postcards from the widespread colonization island. *Nature reviews. Microbiology* 5(5):363-375.
50. Shime-Hattori A*, et al.* (2006) Two type IV pili of Vibrio parahaemolyticus play different roles in biofilm formation. *FEMS Microbiol Lett* 264(1):89-97.
51. Craig L, Pique ME, & Tainer JA (2004) Type IV pilus structure and bacterial pathogenicity. *Nature reviews. Microbiology* 2(5):363-378.
52. Johnston I*, et al.* (2021) Identification of essential genes for Escherichia coli aryl polyene biosynthesis and function in biofilm formation. *NPJ Biofilms Microbiomes* 7(1):56.
53. Kuraishi T, Hori A, & Kurata S (2013) Host-microbe interactions in the gut of Drosophila melanogaster. *Front Physiol* 4:375.
54. Ha EM, Oh CT, Bae YS, & Lee WJ (2005) A direct role for dual oxidase in Drosophila gut immunity. *Science* 310(5749):847-850.
55. Nougayrede JP*, et al.* (2006) Escherichia coli induces DNA double-strand breaks in eukaryotic cells. *Science* 313(5788):848-851.
56. Cuevas-Ramos G*, et al.* (2010) Escherichia coli induces DNA damage in vivo and triggers genomic instability in mammalian cells. *Proc Natl Acad Sci U S A* 107(25):11537-11542.
57. Arthur JC*, et al.* (2012) Intestinal inflammation targets cancer-inducing activity of the microbiota. *Science* 338(6103):120-123.
58. Mougous JD*, et al.* (2006) A virulence locus of Pseudomonas aeruginosa encodes a protein secretion apparatus. *Science* 312(5779):1526-1530.
59. Coyne MJ & Comstock LE (2019) Type VI Secretion Systems and the Gut Microbiota. *Microbiol Spectr* 7(2).
60. Coulthurst S (2019) The Type VI secretion system: a versatile bacterial weapon. *Microbiology (Reading)* 165(5):503-515.
61. Monjaras Feria J & Valvano MA (2020) An Overview of Anti-Eukaryotic T6SS Effectors. *Front Cell Infect Microbiol* 10:584751.
62. Steele MI & Moran NA (2021) Evolution of Interbacterial Antagonism in Bee Gut Microbiota Reflects Host and Symbiont Diversification. *mSystems* 6(3).
63. Powell E, Ratnayeke N, & Moran NA (2016) Strain diversity and host specificity in a specialized gut symbiont of honeybees and bumblebees. *Mol Ecol* 25(18):4461-4471.
64. Pan J*, et al.* (2018) Integration Host Factor Modulates the Expression and Function of T6SS2 in Vibrio fluvialis. *Frontiers in microbiology* 9(962).
65. Chen X, Yu C, Li S, Li X, & Liu Q (2018) Integration Host Factor Is Essential for Biofilm Formation, Extracellular Enzyme, Zeamine Production, and Virulence in Dickeya zeae. *Molecular Plant-Microbe Interactions®* 32(3):325-335.

66. Nikolayeva O & Robinson MD (2014) edgeR for differential RNA-seq and ChIP-seq analysis: an application to stem cell biology. *Methods Mol Biol* 1150:45-79.
67. Robinson MD & Oshlack A (2010) A scaling normalization method for differential expression analysis of RNA-seq data. *Genome Biology* 11(3):R25.
68. Wagner GP, Kin K, & Lynch VJ (2012) Measurement of mRNA abundance using RNA-seq data: RPKM measure is inconsistent among samples. *Theory Biosci Theor Den Biowissenschaften* 131.
69. Freese NH, Norris DC, & Loraine AE (2016) Integrated genome browser: visual analytics platform for genomics. *Bioinformatics* 32(14):2089-2095.
70. Kesnerova L*, et al.* (2019) Gut microbiota structure differs between honeybees in winter and summer. *The ISME journal*.
71. Schneider CA, Rasband WS, & Eliceiri KW (2012) NIH Image to ImageJ: 25 years of image analysis. *Nat Methods* 9(7):671-675.
72. Ducret A, Quardokus EM, & Brun YV (2016) MicrobeJ, a tool for high throughput bacterial cell detection and quantitative analysis. *Nat Microbiol* 1(7):16077.
73. Elso CM*, et al.* (2004) Leishmaniasis host response loci (lmr1-3) modify disease severity through a Th1/Th2-independent pathway. *Genes Immun* 5(2):93-100.
74. Martinez-Garcia E*, et al.* (2020) SEVA 3.0: an update of the Standard European Vector Architecture for enabling portability of genetic constructs among diverse bacterial hosts. *Nucleic acids research* 48(6):3395.
75. Harms A*, et al.* (2017) A bacterial toxin-antitoxin module is the origin of inter-bacterial and inter-kingdom effectors of Bartonella. *PLoS Genet* 13(10):e1007077.
76. Deatherage DE & Barrick JE (2014) Identification of mutations in laboratory-evolved microbes from next-generation sequencing data using breseq. *Methods Mol Biol* 1151:165-188.
77. Guy L, Kultima JR, & Andersson SG (2010) genoPlotR: comparative gene and genome visualization in R. *Bioinformatics* 26(18):2334-2335.
78. Zufelato MS, Lourenço AP, Simões ZL, Jorge JA, & Bitondi MM (2004) Phenoloxidase activity in Apis mellifera honey bee pupae, and ecdysteroid-dependent expression of the prophenoloxidase mRNA. *Insect biochemistry and molecular biology* 34(12):1257-1268.